Final Report to OEER/OETR for

Assessment of the Potential of Tidal Power from Minas Passage and Minas Basin

Project Number: 300-170-09-11
Research time frame: October, 2009 to September, 2011

Richard Karsten,
with
Joel Culina, Amanda Swan, Mitchell O'Flaherty-Sproul, Amber Corkum
Department of Mathematics and Statistics, Acadia University
David Greenberg
Bedford Institute of Oceanography, Fisheries and Oceans Canada
and
Michael Tarbotton
Triton Consultants Ltd.

Submitted November 20, 2011

Summary

This research project was undertaken to accurately estimate the power potential of the tides and tidal currents in the Minas Basin and Minas Channel regions of the Bay of Fundy. Its goal was to make a power estimate that is both attainable and sustainable; that is, an assessment based on available turbine technology that includes an estimate of the impact on the tidal range and currents. The results of our theoretical analysis and hydrodynamic modelling are producing critical information for many stakeholders. For developers, it will provide realistic power estimates that will determine if commercial scale turbine farms are financially viable. For resource users, it will provide estimates of the changes to the physical environment such power extraction will produce so that they can determine how their livelihood will be affected. For researchers, it will provide the baseline changes to tidal range and currents that will be necessary to examine changes in sediment, impacts on marine life, and other concerns.

The research, described in detail in this report, focused on four topics. First, we examined the improvement of the numerical simulations of the tides and tidal flows in the upper Bay of Fundy. The numerical models, FVCOM and RiCOM, have been run at high resolution in 2D and 3D. The models have been validated against data gathered from ADCPs. This has produced an accurate data set of tidal currents through Minas Passage that will be made publicly available through an ftp site in the coming month. The high resolution simulations has revealed that the flow through Minas Passage is turbulent, with large eddies forming around major bathymetric features. In particular, the slack after the flood tide is dominated by these eddies. The flood and ebb tides are very different, with the flood tide dominated by a strong jet coming off the tip of Cape Split.

Although the models have improved significantly, there is still significant issues that need to be addressed. Observations have shown that the bottom roughness varies across Minas Passage. Observations and simulations show that the throughout the water column is determined by the bottom drag, and therefore accurate modelling of the bottom roughness on the flow is critical. This requires further research. As well, the observations show large velocity fluctuations due to unsteady flow and turbulence. Further work needs to be done to include these in numerical simulations. As well, other effects such as waves and extreme weather events need to be included to get a complete analysis of the variations and extremes of the tidal currents in Minas Passage.

Secondly, we adapted previous theoretical analysis to the specific dynamics of Minas Passage to predict the potential power of turbine fences. This analysis illustrates the importance of the blockage ratio, the portion of the channel cross-section that turbines occupy. If the blockage ratio is high, turbines can be designed to extract significantly more power from the flow. In such cases, the power the turbine fence generates can be over 500% the kinetic energy flux, rather than the 59% maximum of a single turbine. For more realistic smaller blockage ratios, similar large amounts of power can be extracted using many turbine fences. The theory highlights the difference between the power that is available to the turbine for

power generation and the total power extracted from the flow. The extracted power exceeds the generation power because energy is lost in the turbine wake (and due to the drag of the turbine supporting structure). It is the extracted power that determines how much power can be taken from a given tidal flow and how extracting this power will change the tidal flow. It is therefore important to increase turbine efficiency, the ratio of the generated power to the extracted power. However, there is a trade-off between maximizing the generated power and increasing efficiency. For Minas Passage, where we expect blockage ratios are most likely to be less than 20%, the theory suggests that it is still possible for the generation power to be exceed 2500 MW for less than a 5% reduction in the flow, and aprroximately 800 MW for the first 1% reduction in the flow. These results confirm that previous results can be extended to realistic turbine fences.

Our third research topic was the analysis of power extraction using numerical simulations. Using a typical power curve for a 1.2 MW turbine, we used the water speed calculated by our numerical simulations to generate a map of the potential power generation over the Minas Passage. The resulting map shows that there are tens of thousands of locations where the turbine will generate a mean power exceeding 750 kW, a very high capacity factor. This region cover the northern portion of the passage with a significant portion in water depths that exceed 50 m. We also examined the power potential of a 3D complete turbine fence, illustrating that numerical simulations roughly agree with the theory analysis. We did show that increasing the numerical resolution could reduce the maximum power extracted, from 8 GW to 6 GW. This emphasizes that the numbers produced by simulations are not absolute, but will change as the models are adapted and improved. But, significantly, moving to 3D dimensional simulations has not changed qualitatively the 2D results. When we examined partial turbine fences, the simulations suggested that significantly more turbine power than the theory suggested was possible. In the simulations, the turbine drag could be increased to much higher values than the theory suggested. Why this is the case is not fully understood, we believe it is connected to the vertical profile of the flow. It is the focus of ongoing research.

Finally, we combined numerical and theoretical to construct a Turbine Array Model. This model was a relatively simple tool to quickly analyse what the power potential of turbine arrays in Minas Passage. Importantly, included a model of turbine wakes and therefore could assess realistic arrangement of turbines. This model further confirmed previous results. For a small number of turbines, the turbines can theoretically generate in excess of 1MW each. As the number of turbines increases, the turbines must be placed in locations of slower flow and will produce less power. This is especially true if the turbines are restricted to shallow water, for example if the turbines are restricted to water less than 50 m less than 500 turbines can be reasonably located. For all the tested arrays, the model suggests that about 800 MW of power is available for each 1% reduction in the flow through Minas Passage. Even given the reduction in efficiencies of real turbines, this suggests that hundreds of turbines producing hundreds of MW will results in a minimal, likely difficult to observe, reduction in flow through Minas Passage.

In conclusion, our research has supported previous results that in the range of 2000 MW of power extracted from Minas Passage by an array of in-stream tidal turbines with a relatively

small reduction in the flow through the passage, less than 5%. For smaller arrays, the turbines can be placed in locations with the fastest water and produce power more efficiently with even less impact. Of course, these are initial estimates. More work remains to be done to understand the turbulent nature of tidal flow, the complex interaction of turbines and the flow, and possibility of designing turbines to make arrays generate electricity with minimum power extraction.

Contents

List of Figures

List of Tables

Chapter 1

Introduction

The Bay of Fundy has the world's highest tides, reaching over 6 m in amplitude in Minas Basin. The basin is connected to the Bay of Fundy by Minas Passage, a channel that is roughly 5 km wide, 15 km long, and up to 150 m deep (see Fig. 2.1). During flood and ebb tide the water flux through the passage can reach 1×10^6 m^3 s^{-1} with water speeds exceeding 5 m s^{-1}. These high water speeds and the huge volume of water flowing through the passage make it one of the world's most interesting sites for instream tidal power development. Currently, the Nova Scotia Department of Energy is spearheading a project to deploy test turbines in Minas Passage to explore the possibility of further commercial development.

A critical aspect of tidal power development is an accurate assessment of the power resource. Initial assessments of Minas Passage, based on estimates of the kinetic energy flux through the passage, estimated a maximum power of 1.9 GW [1]. From this maximum power, it is often estimated that less than 15% of the power would be available for electricity generation, giving an estimate of roughly 170 MW of generation capacity for Minas Passage and roughly 300 MW for the entire Minas Channel [2]. These estimates are considerably smaller than the 10-GW estimate based on the mean potential energy of the tides in Minas Basin [3]. This difference would suggest that tidal barrages or lagoons may be a better mechanism to take advantage of the power in the tides. But before we discount the idea of instream turbines, it is important that we carefully examine their potential.

A more recent assessment of the power potential of Minas Passage was presented in Karsten, McMillan, Lickley, and Haynes [4], hereafter KMLH. KMLH adapted the results of [5] to the case of a channel connecting a tidal basin to the ocean. They derived a formula for the maximum extractable mean power given by

$$P_{\text{avg}} \approx 0.2 \rho g a Q_0 \,, \tag{1.1}$$

where ρ is the water density (taken to be 1025 kg/m^3), a is the amplitude of the forcing tides at the entrance of the channel, g is the acceleration due to gravity, and Q_0 is the maximum volumetric flow rate through the channel in the undisturbed state (see also [6] for more details regarding this formula). The formula in Equation 1.1 includes the tidal forcing through a and depends linearly on the current speed through the flow rate, Q_0. As well, since the power depends on the volumetric flow rate, the formula does not differentiate between

thin channels with strong flow and wide channels with weaker flow. It should be emphasized that for a channel connected to a basin, the potential power does not depend on the existing tidal head across the channel, which is often small, but on the potential tidal head—the tidal head when the forcing tides and basin tides are 90 degrees out of phase. From our numerical simulation, we find that for Minas Passage $a = 4.5$ m and $Q_0 = 8.4 \times 10^5$ m^{3}s^{-1}, giving a maximum, time-mean, extractable power of $P_{avg} = 7400$ MW!

KMLH applied the theory to Minas Passage and compared it to a 2D, depth-averaged numerical model of the tidal flow in the Bay of Fundy. The numerical model extracted power from Minas Passage by increasing the bottom friction in the passage. They illustrated that the theory agreed well with numerical simulations, both in terms of the power that can be extracted and the impact of the power extraction on the flow through Minas Passage. The maximum mean extractable power was calculated to be nearly 7000 MW. The impact of extracting this much power was a 40% reduction in the flow through Minas Passage and a similar reduction in the tides in Minas Basin. As well, KMLH also demonstrated that any power extraction in Minas Passage pushes the Bay of Fundy–Gulf of Maine system closer to resonance with the forcing tides, resulting in increased tidal amplitudes throughout the Gulf of Maine. When 7000 MW of power was extracted, these increases in the tides could be as large as 20%. While extracting the maximum power produces significant impacts, these impacts were reduced dramatically if the extracted power was reduced. KMLH calculated that 2500 MW of power can be extracted with a maximum 5% change in the tidal amplitude throughout the Bay of Fundy and the Gulf of Maine, with the largest changes in Minas Basin.

The ability to extract such a large amount of power without drastically reducing the flow is related to the increase in the tidal head across the passage as power is extracted. In the KMLH numerical simulations of Minas Passage, the tidal head increases from 1.4 m to 3.2 m as more power is extracted from the passage. This increase in the tidal head increases the hydrostatic pressure that forces the flow through the passage, partially offsetting the retarding force of the turbines. It should be noted that it is critical to limit the reduction in flow through the passage because this reduction in flow directly translates into a reduction in the tidal range in the Minas Basin. Even small changes in the tidal range could have a severe impact on the sensitive and important intertidal ecology of the basin.

The objective of our research was the primary research objective of this OEER/OETR call for proposals: the accurate assessment of the potential power resource of the upper Bay of Fundy, in particular the Minas Passage, using hydrodynamic models. As part of this assessment, the research addressed the accurate modelling of the tides and tidal currents in the region, the modelling of the extraction of power from the tides using both in-stream tidal turbines, and the estimation of the impact power extraction will have on the tides and currents throughout the region. As such, it also addresses such fundamental issues as site selection, economic feasibility, and environmental impact.

The results of KMLH were important in illustrating that it is possible to extract significant amounts of power from Minas Passage currents. However, these estimates were based on turbines that essentially constituted a barrage where all the water flowing through the

passage flows through the turbines. Thus, while the calculations in KMLH can be seen as useful bounds on the power extraction, it is not clear how they apply to realistic arrays of individual turbines. Assessing arrays of turbines using full numerical simulations can be difficult, with computational costs that are prohibitive. Accurately representing turbines in a coastal ocean model requires such a high resolution that the time step used must be extremely small. Consequently, running a single simulation can be extremely costly. Such models are not suitable to examine the variation of the turbine characteristics or to optimize the placement of individual turbines.

In order to complete our research, we brought together several important resources: experienced modellers who have worked in modelling the Bay of Fundy and worked on tidal power, numerical models that can be adapted to answer the questions at hand, computational resources on which to run the models, and young researchers to run the models and compile the results. The project investigators have the considerable experience with modelling tidal flows and tidal power in the Bay of Fundy and elsewhere. In particular, Dr. Walters is the creator of RiCOM and therefore brings considerable expertise to this research. The group used two numerical models, FVCOM (see Chen et al. 2006) and RiCOM (Walters 2005), that have shown to be suitable to examine the problem. These models each have their own strengths, and the use of two models will allow the appropriate model to be used for different aspects of the problem while also allowing for the cross validation of the results. For most of the results we used the computational resources available at Acadia through the Acadia Centre for Mathematical Modelling and Computation (ACMMaC) and the Atlantic Computational Excellence Network (ACEnet). Finally, the project benefited from the considerable research expertise of the young researchers who joined the project, namely Dr. Joel Culina, MSc candidate Mitchell O'Flaherty Sproul, and undergraduate students Amanda Swan, Amber Corkum and Michael Deveau.

As outlined in the next chapter, our research addressed several issues. First we developed an accurate model of tidal currents and tides in the Minas Channel and Basin. Second, we used analytical theories to assess the tidal resource in Minas Passage. Third, we used numerical simulations with modelled turbines to test the theoretical assessments. And, finally we developed a model of tidal turbine arrays. In this report, we also describe our efforts to disseminate the results of our analysis to all stakeholders, and our work with technology developers and researchers to examine the potential and impact of tidal energy.

Chapter 2

Research Description

2.1 Modelling the flow through Minas Passage

While the previous numerical modelling of the flow through Minas Passage resulted in encouraging benchmarks (see [4], they do not address questions on scales of individual TISEC devices. For reasons including limits on computational speed, Computational Fluid Dynamics (CFD) models that can (in theory) model at the smallest scales of fluid motion cannot (presently) be used to model the larger-scale flows with which the turbines will interact. Rather, a hierarchy of 'nested' models of increasing resolution and sophistication is needed to address problems from the array/turbine-farm scale down to the turbine blade scale. By nesting, it is meant that the models at different scales mutually interact. For example, a Reynolds-averaged Navier-Stokes (RANS) model of the ensemble-mean flow would provide boundary values for a CFD model of an individual turbine, which, in turn, would be used to parameterise its effect in the RANS model.

As a step towards creating a hierarchy of models of the Bay of Fundy, our research is concerned with the hydrodynamic changes that arise as a result of increasing the model resolution in the Minas Passage. In particular, RANS models with different resolution grids are compared against each other and against observations. This comparison involves use of a set of turbine-relevant metrics which illuminate differences in bottom/sea-bed stress between the models and observations and a diminished current speed with increased resolution.

In this study we use the Finite Volume Coastal Ocean Model (FVCOM) [7]. The important features of the model and complete details of the model simulations discussed here are found [8].

The model domain, shown in Fig. 2.1, covers the upper portion of the Bay of Fundy. Fig. 2.1 also shows the bathymetry used in the simulations, and specifically the bathymetry in Minas Passage.

The model domain is delineated by a land boundary to the north, south and east, and to the west by an open boundary, which is (arbitrarily) defined by a line across the lower Bay of Fundy roughly connecting Saint John, New Brunswick to Digby, Nova Scotia. The model is forced entirely by specifying tidal (elevation) constituents at the open boundary, among

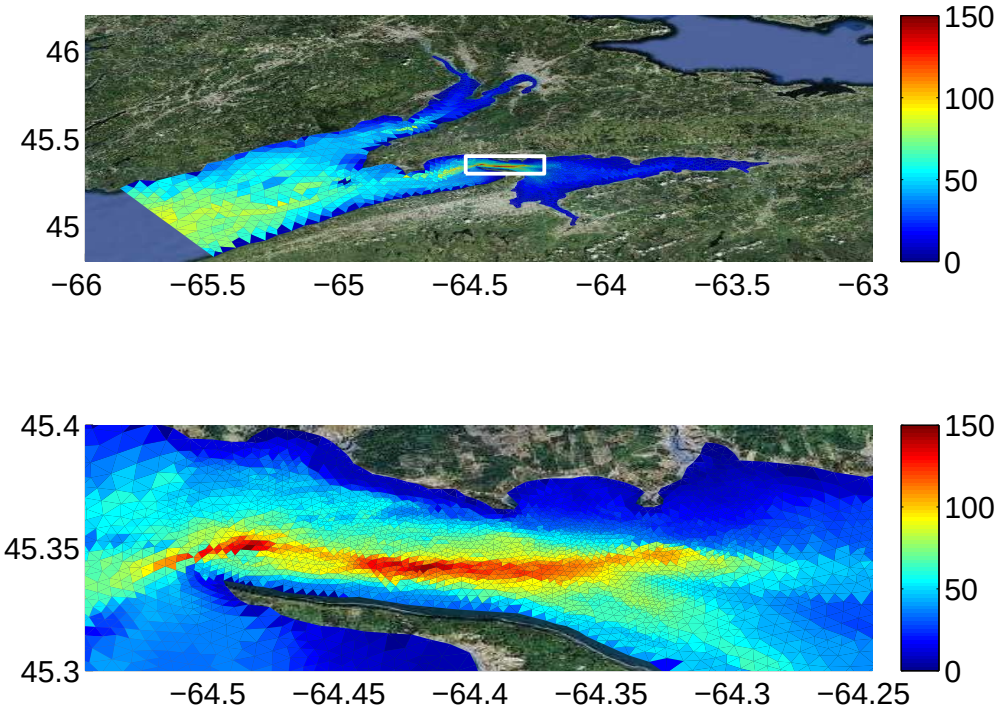

Figure 2.1: The upper bay of fundy region modelled in the numerical simulations. the contours show the numerical grid and the colours show the water depth. minas passage is the region in the white box and is shown in detail in the lower graph.

which the dominant constituent is the lunar, semi-diurnal M_2 constituent (with period$\approx$ 12.42 hr).

The results of [4] were derived using FVCOM with an unstructured grid consisting of triangles of varying size. The grid had relatively low resolution and is hereafter called 'lr-grid'. The greatest density of triangles in the lr-grid is located in the region of interest, Minas Passage, with triangles with sides that are $200 - 300$ m long. Although this length-scale is much larger than associated with individual turbines, this resolution is sufficient for determining power potential through the use of turbine fences spanning a cross-section of the channel. However, as scales of interest decrease, finer grids are required to resolve not only the activity surrounding turbines but also finer-scale flow features, such as prominent 3D eddies in Minas Passage, that exist without the presence of turbines. The lr-grid is compared to a higher resolution grid ('hr-grid'), which was created independently of the lr-grid. The hr-grid has a roughly similar distribution of triangles, with a concentration of triangles in Minas Passage, but the triangle sides in this region have lengths between 60 and 80 metres. The differences between the meshes are illustrated in Fig. 2.2.

The scales that can be resolved by the hr-grid are about as fine as possible with the version of FVCOM used in this paper. Specifically, the hydrostatic assumption, which reduces the vertical transport equation to a balance between the vertical pressure gradient and gravity, and the turbulent-viscosity representation of the Reynolds stresses filter out vertical (and horizontal) motions that are important in the vigorously mixing waters of Minas Passage. The non-hydrostatic version of FVCOM has shown some success in modelling idealised situations at $\mathcal{O}(10$ m) scales [9]. However, it is not yet computationally feasible (nor possibly even tractable) to run the non-hydrostatic version of FVCOM over domains as large and refined as the ones considered in this paper.

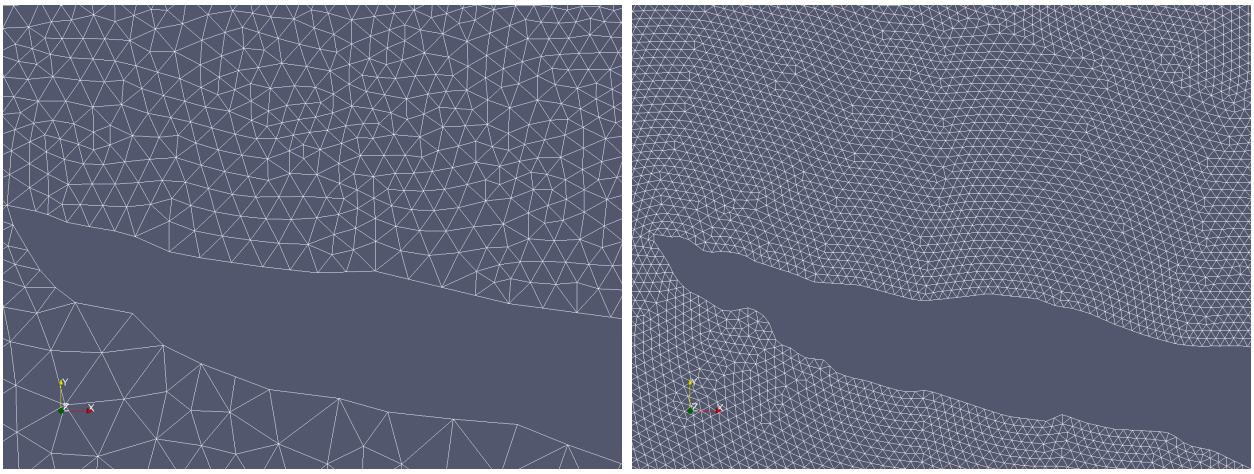

Figure 2.2: The low-resolution (top) and high-resolution (bottom) grids over the waters surrounding Cape Split (see Fig. 2.3). The two images depict the same surface area ($\mathcal{O}(200$ km^2). The resolution of the hr-grid is approximately fives times that of the lr-grid.

FVCOM with lr-grid was previously calibrated in [10] against observed tidal height and

current velocity constituents. The tuning primarily involved adjustment of the bottom friction input parameter $C_{D(input)}$, which determines the values of bottom stress (this is elaborated on in Section **??**)). To determine the effect of resolution, the same parameters are used to run both the low and high resolutions models; namely, those parameters by which the low resolution model is calibrated to observations. These different resolution models are compared against each other and against the latest Acoustic Doppler Current Profiler (ADCP) measurements in Minas Passage. In comparison to the observed tidal velocity (and height), this set-up favours the low-resolution model over the high-resolution model, but additional metrics besides velocity are considered in determining the performance of the models. Generally, it is expected that there will be a convergence of the (statistics of) the large-scale hydrodynamics with increasing resolution.

ADCPs were deployed at six locations in the Minas Passage for durations of at least 28 days over the Winter and Summer of 2009 (Fig. 2.3). The ADCPs measured the current velocities through the water column above the Profilers, ensemble averaging the data over 1 minute intervals.

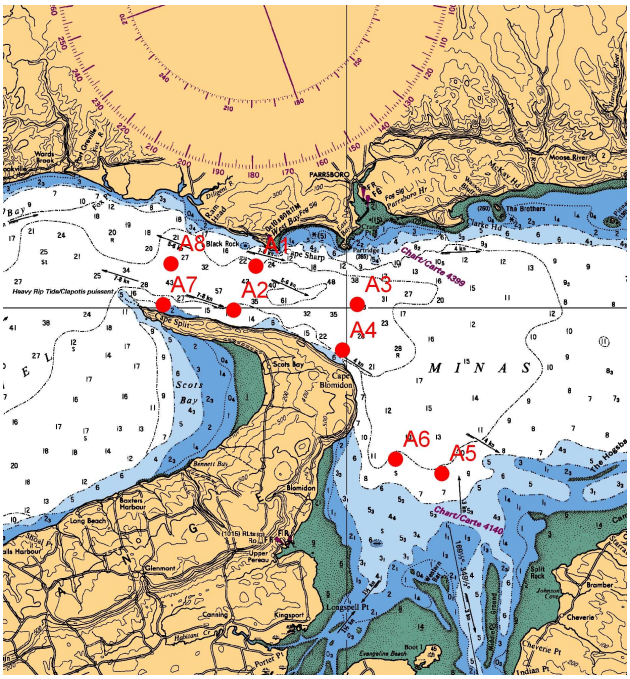

Figure 2.3: The positions of the Acoustic Doppler Current Profilers (ADCPs) deployed during the Winter and Summer of 2009. The ADCPs of interest in Minas Passage (A1, A2, A3, A4, A7 and A8) recorded current measurements for at least 28 days.

In Fig. 2.4, we compare the time series for the observed data The numerical simulation does a reasonable job at capturing the amplitude and phase of the speed. It captures the pulse in flow at the beginning of ebb tide (for example at hour 260). This feature is connected to an eddy formed in West Bay being advected out into the passage at the beginning of the

ebb tide, see Fig. 2.12. The model does not capture the high frequency fluctuations seen in the ADCP data.

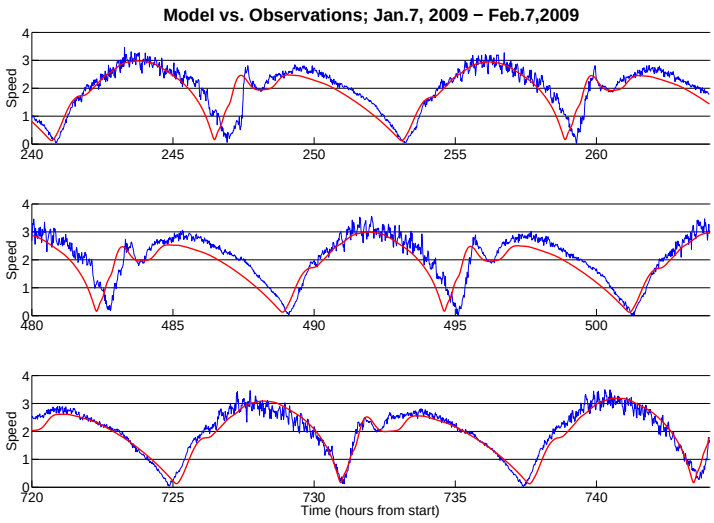

Figure 2.4: A comparison of simulated water speed (red) and observed water speed at location A1 for January 2009.

The ADCP data and corresponding model data are analysed using turbine-relevant metrics based on [11, 12] and [13], and are presented in Tables 2.1–2.3. Measurements are taken at the vertical bin (or at the vertical level in the case of the models) closest to a projected turbine hub-height above the sea bed of 15 metres. Details of the table entries are discussed in [8].

In general, the metrics for the observed and modelled velocities agree reasonably well given that the numerical models were not tuned to these observations. There are significant differences, for example in the direction of flow at site A7. This site sits in the recirculation zone along Cape Split and therefore the direction of flow is a difficult to measure and model correctly. There are two key differences between models and observations that we will discussed in more detail:

1. Modelled C_D, and hence modelled bottom stress, is (almost) spatially homogeneous whereas the observed values vary significantly in space.

2. The current speed is significantly lower on the high-resolution grid compared to the low-resolution grid.

In calibrating FVCOM with the lr-grid, $C_{D(input)}$ was set to a value much higher than for a level, smooth bed. This large value appears to be justified as the observed values of bottom friction coefficient are similarly large. Large values of C_D are consistent with a seabed that

Table 2.1: Summary of FVCOM simulations of Minas Passage using low (lr) and high (hr) resolution grids (A1–A2)

Site	Obs-A1	lr-A1	hr-A1	Obs-A2	lr-A2	hr-A24
Velocity						
Mean speed (m/s)	1.85	1.83	1.58	1.25	1.09	0.96
Max sustained speed (m/s)	3.41	3.31	2.93	3.14	2.57	2.50
Ebb/flood asymmetry	0.93	1.03	1.03	1.27	1.59	1.19
Shear stress (Nm^{-2})	23.8	27.9	21.1	12.1	14.2	12.4
Power						
Mean kinetic power density (kW/m^3)	4.79	4.64	2.97	1.84	1.45	0.97
Kinetic power asymmetry	0.80	1.08	1.11	2.32	3.60	2.02
Direction						
Principal direction $(deg\ CW\ from\ N)$	-72	-74	-73	-77	-78	-78
Directional deviation (deg)	9	6	8	8	8	9
Directional asymmetry (deg)	9	9	9	16	17	14
Vertical Profile						
Bottom friction coeff. $C_D(\overline{u}) \times 10^{-3}$	5.0	6.5	6.5	3.2	5.4	5.1
% of column occupied by log-layer	90%	68%	80%	80%	58%	49%
Specs						
Assumed hub height above sea bed (m)	15	15	15	15	15	15
Mean depth of water column (m)	50	57	52	50	53	53

is very rough and/or characterised by bedforms, which induce form drag in the water above [13].

However, the modelled C_D does not vary significantly among locations (reflecting that $C_{D(input)}$ was set to be spatially constant), whereas there is significant spatial heterogeneity in the observed bottom stress. For example, the observed bottom friction coefficient at mooring A8 is almost 2.5 times larger than at A3. Since A8 and A3 roughly coincide with the path taken by the flow during flood and ebb tides, a parcel of water (sufficiently close to the bottom) is subject to significantly different bottom drag while flowing through Minas Passage. This heterogeneity in values of the bottom friction coefficient is consistent with the heterogeneity observed in values of bottom roughness height inferred from grain size distribution in the Bay of Fundy [10].

In the standard formulation, the velocity in the logarithmic layer scales as the bottom friction velocity. It is a striking feature from observations, and a feature mostly captured by the models, that the logarithmic layer reaches far up the water column. It has been shown in [13] that the logarithmic layer in a tidal boundary layer is proportional to u_*/ω, where ω is the angular frequency of the tide. Since in Minas Passage the bottom friction velocity is very large and the semi-diurnal M_2 tidal constituent dominates, the size of the logarithmic layer is consistent with these scaling arguments.

As a result of the large logarithmic layer, the effects of bottom stress in the Minas Passage during ebb and flood tides extend through most of the water column, acting to reduce the

Table 2.2: Summary of FVCOM simulations of Minas Passage using low (lr) and high (hr) resolution grids (A3–A4)

Site	Obs-A3	lr-A3	hr-A3	Obs-A4	lr-A4	hr-A4
Velocity						
Mean speed (m/s)	1.39	1.40	1.09	1.49	1.30	1.20
Max sustained speed (m/s)	3.00	3.02	2.35	3.24	2.82	2.48
Ebb/flood asymmetry	0.82	0.82	0.87	1.28	1.37	1.30
Shear stress (Nm^{-2})	9.7	17.2	13.1	17.1	17.3	14.0
Power						
Mean kinetic power density (kW/m^3)	2.31	2.45	1.12	2.83	2.09	1.51
Kinetic power asymmetry	0.57	0.52	0.64	2.16	2.58	2.17
Direction						
Principal direction $(deg\ CW\ from\ N)$	-79	-78	-78	-57	-59	-57
Directional deviation (deg)	5	5	4	7	2	4
Directional asymmetry (deg)	9	5	4	12	2	4
Vertical Profile						
Bottom friction coeff. $C_D(\overline{u}) \times 10^{-3}$	2.5	5.3	5.4	4.2	5.0	5.6
% of column occupied by log-layer	74%	76%	69%	83%	65%	6%
Specs						
Assumed hub height above sea bed (m)	15	15	15	15	15	15
Mean depth of water column (m)	52	56	55	47	50	49

current speed through most of the water column. To further justify this point, the shear stress and eddy viscosity through the water column at the ADCP locations are deduced based on the assumptions that a) the flow is rectilinear; b) shearing stresses on a vertical plane are negligibly small; c) the vertical components of velocity and acceleration may be neglected; d) conditions in the horizontal are sufficiently uniform in the horizontal directions for advection terms to be neglected; and e) the density of water is uniform [14]. Applying these assumptions, and additionally assuming that the profile is logarithmic, eddy viscosity profiles are computed and shown for A8 in Figure 2.5 (additionally, the values of shear stress at hub height are given in Table **??**). The eddy viscosity profiles are particularly revealing as to the reach of the logarithmic layer. The modelled viscosity profiles, determined by a set of partial differential equations, agree with those generated by Prandtl's diagnostic mixing-length formulation of eddy viscosity ν_T:

$$\nu_T = \kappa u_* z(1 - z/h), \tag{2.1}$$

where u_* is the bottom friction velocity, $\kappa = 0.41$ is the von Kármán constant, z is the height above the sea bed and h is the water depth. Since in Prandtl's equation (2.1) the viscosity profile through the water column scales as the bottom friction velocity, the friction velocity/bottom stress similarly impacts the current speed through the water column.

It is thus very important that the bottom stress be accurately specified in modelling the flow through Minas Passage. However, the flow in Minas Passage is determined locally by

Table 2.3: Summary of FVCOM simulations of Minas Passage using low (lr) and high (hr) resolution grids (A7–A8)

Site	Obs-A7	lr-A7	hr-A7	Obs-A8	lr-A8	hr-A8
Velocity						
Mean speed (m/s)	0.97	1.10	1.18	1.78	2.21	1.75
Max sustained speed (m/s)	1.96	2.73	2.73	3.50	4.95	4.04
Ebb/flood asymmetry	2.82	3.02	2.40	0.66	0.65	0.66
Shear stress (Nm^{-2})	4.2	10.2	8.2	41.8	28.5	20.3
Power						
Mean kinetic power density (kW/m^3)	0.72	1.58	1.43	4.94	10.09	5.05
Kinetic power asymmetry	16.59	35.42	12.58	0.29	0.26	0.25
Direction						
Principal direction $(deg\ CW\ from\ N)$	245	-69	-76	-78	-79	-79
Directional deviation (deg)	6	8	11	12	9	13
Directional asymmetry (deg)	5	13	3	2	11	10
Vertical Profile						
Bottom friction coeff. $C_D(\overline{u}) \times 10^{-3}$	4.7	6.4	5.9	6.0	5.3	5.4
% of column occupied by log-layer	87%	98%	89%	82%	96%	97%
Specs						
Assumed hub height above sea bed (m)	15	15	15	15	15	15
Mean depth of water column (m)	35	39	37	67	71	66

more than the bottom boundary values. This is evident from the reduction in current speeds with increased resolution (cf. Tables 2.1–2.3) despite the similarity of the bottom stress over the two grids.

The ADCP (point) measurements offer a glimpse of the power contained in the Minas Passage. Models show current speed and hence (modelled) power over the entire domain of interest, limited only by resolution. However, it is evident from the modelled point measurements that higher resolution offers more than a more detailed picture; it also affects the hydrodynamics in the Minas Passage as manifest by a significant reduction in current speed.

Over the Minas Passage, there are clearly differences between the spatial distributions of the ebb-tide and flood-tide currents. On coarse scales, the spatial distribution of the ebb-tide current is uniform through the Minas Channel. On flood-tide, however, there is a well-defined region of relatively slowly-moving, eddying flow, bounded towards the Channel centre by a narrow 'jet' (cf. Fig. 2.7). The current speed slowly diminishes moving northwards from the jet. The large eddying region and the associated jet, characterised by large spatial gradients in current speed and direction, are expected to be sensitive to model resolution (and other parameter) changes, and are thus here examined towards understanding the reasons for diminished current speed with increased resolution.

Fig. 2.6 depicts a map of the difference in power density generated over two different

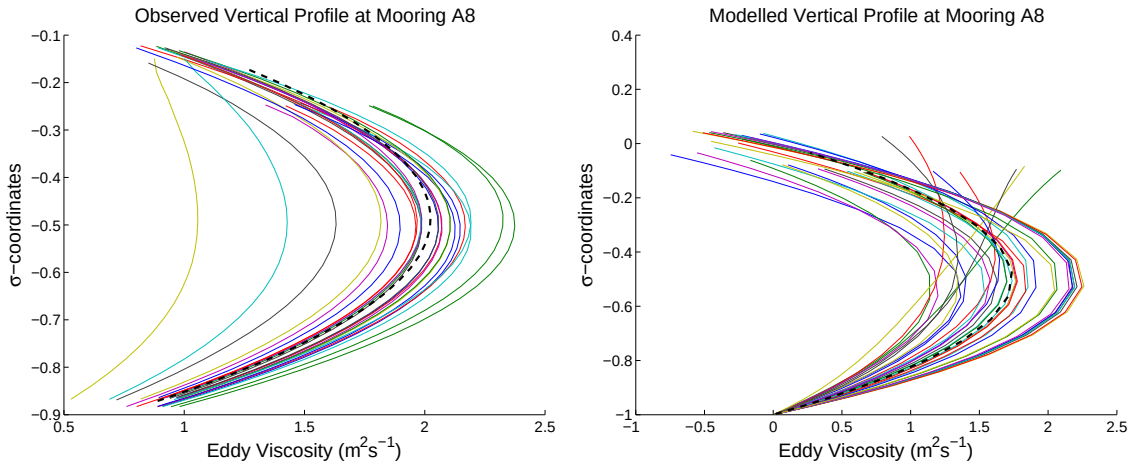

Figure 2.5: The observed (left) and modelled (right) profiles of vertical eddy viscosity for strong ebb and flood tides over one day. The model result is from FVCOM with lr-grid. The black dotted line is the eddy viscosity based on the mixing-length formulation given by $\nu_T = \kappa\overline{|u_*|}z(1 - z/h)$, where the average is taken over observed friction velocities.

resolution grids (otherwise the parameters are the same). Power is significantly reduced over the high-resolution grid through the fastest-flowing regions, with a maximum absolute difference in power density (i.e., kinetic energy flux density) of 20 kW/m^2. This latter value corresponds to a reduction in current speed by a factor of about 1/4.

Despite reductions in the speed of the currents, their directional properties do not appear to be as sensitive to changes in resolution. At the ADCP locations in particular, there is excellent agreement between the different resolution grids concerning the direction of the principal axes (which also agree very well with observations, except at location A7 where eddy activity is intense). On broader scales, it is evident from Fig. 2.6 that the two distributions of power, over the two grids, are (grossly) similar.

A closer look at the flood-tide jet reveals just how little the jet position depends on resolution. The jet is a well-defined feature in both grids, with a narrow hump in current speed against cross-sectional position along most of the Minas Passage clearly marking its position. From the jet to the eddying region, there is a sharp, monotonic decrease in the current speed, representing the region of entrainment of the slower eddying flow into the jet region. The jet axis and the jet half-radius associated with the high and low resolution grids are depicted in Fig. 2.7. The jet axis position corresponds to the position of current speed maximum values, found over a succession of cross-channel transects. The jet half-radius is determined by locating the position to the south of the jet at which the current is half the velocity at the jet centre-line/axis.

Through much of the Minas Passage the high and low resolution jet axes are nearly coincident. On the high-resolution grid, towards the channel exit on the Minas Basin side, the global maximum speed (along transects) shifts to a near-shore position, but there remains a local, although diminished and less well-defined, maximum along the (mid-Channel) jet

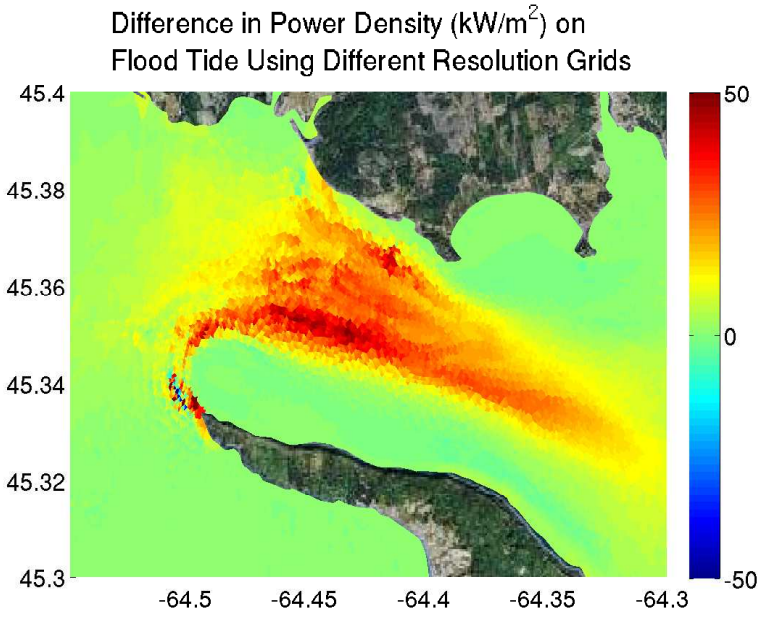

Figure 2.6: Power density on flood tide with low-resolution grid subtracted from that with high-resolution grid.

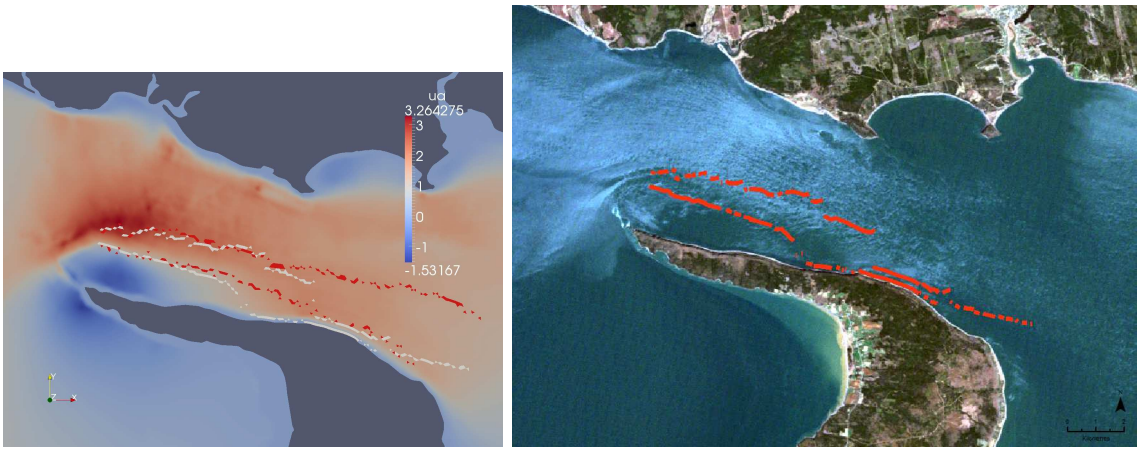

Figure 2.7: Left: the modelled flood-tide jet at an instant in time (May 20, 2004). The white lines are generated on the high-resolution grid and the red lines on the low-resolution grid. The lines closer to mid-Channel are the jet centre-lines and to the south are the jet half-lines. The background colouring is the east component of the depth-averaged speed on the high-resolution grid. Right: The high-resolution grid jet lines overlaid onto the corresponding Landsat satellite image.

trajectory. It is expected that the jet will diminish as the channel empties into the Basin. On the low-resolution grid, there is also a decrease in jet speed and increase in near-shore current speed, but the near-shore speeds remain smaller than the mid-Passage values much further into the Basin.

The bottom image in Fig. 2.7 shows a Landsat optical satellite image of Minas Passage with the high-resolution grid jet axis and jet half-radius overlaid. The satellite image is marked by the presence on the sea-surface of white streak lines, including one opaque, thick, well-delineated streak line north-west of Cape Split which connects to the overlaid image of the modelled jet centre-line. The nature and relation of these streak lines (possible wave foam-lines) to the hydrodynamics is unknown, but if the thick streak line is presumed to correspond to the path of the jet, then the models do an excellent job in capturing the observed position of the the jet in this region. These images are compelling, and Radarsat images will be examined in a future study to determine if the jet path can be quantitatively tracked.

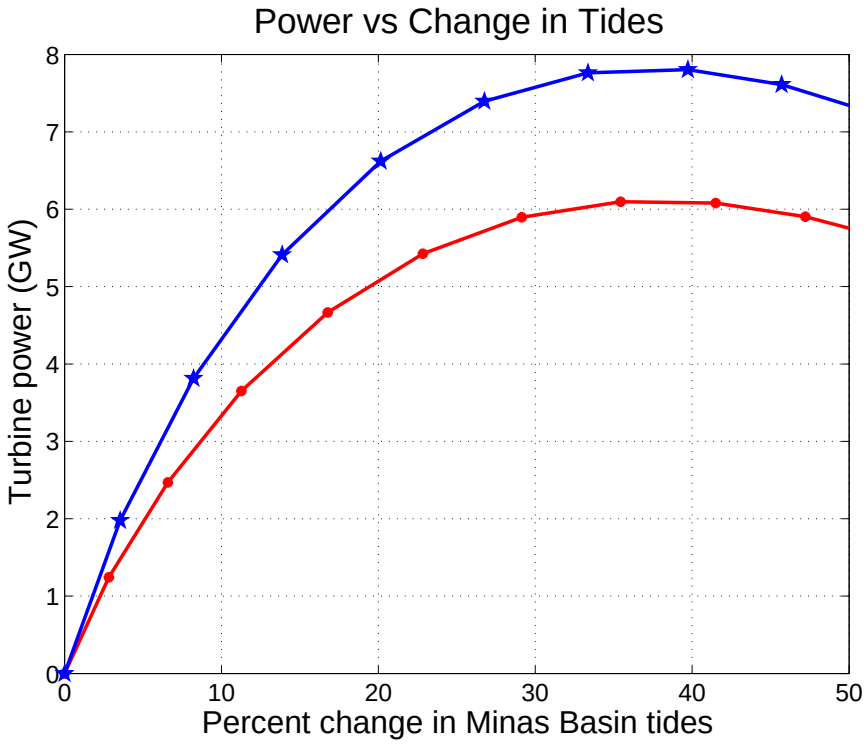

Figure 2.8: Extractable power averaged over a tidal cycle as a function of the change in tidal height using the low-resolution grid (star, blue) and high-resolution grid (circle, red). Power is extracted by applying a constant drag over a full cross-section of Minas Passage, representing a full turbine fence spanning the Passage, a set-up that maximises the power that can be extracted. A greater percent change in tidal height corresponds to an increased value of drag.

Of course, the reduction in power with increased resolution has important implications

for resource assessment. The broadest question concerning the quantity of extractable power in the Minas Channel is answered in [4]. Using a 2D model, they modelled a full fence of turbines by increasing bottom friction at all grid-points on a cross-section of the channel. We repeat their calculation here with the two different resolution grids. The results are shown in Fig. 2.8. With FVCOM with hr-grid, the maximum extractable power decreases to 6 GW, as would be expected with the lower water speeds. Otherwise, the conclusions of [4] remain, a large amount of power can still be extracted with a minimal decrease in tidal height. However, the drag at which the maximum power is extracted is greater with the high-resolution grid compared to the low-resolution grid. This fact, and the fact that less power is extracted with the high-resolution grid, are both consistent with the presence of a higher natural drag in the Minas Passage; i.e., the increased resolution is causing a greater drag on the flow through the Passage. The Garrett-Cummins theory in fact has a tunable, natural drag parameter, from which it may be deduced that $6 - 8$ GW of power can be extracted, in agreement with the results here presented.

The modelled currents through Minas Passage are shown in Figs. 2.9 and 2.10. Fig. 2.9 shows the depth-averaged water speed through Minas Passage at flood and ebb tide. There is a significant asymmetry between the flood and ebb tides. During flood tides the flow around Cape Split (the peninsula at the bottom of the figure) results in a very strong jet in the northern half of the passage, with a weak return flow along Cape Split. During ebb tide the flow is weaker and almost evenly spread across the passage. Fig. 2.10 shows a cross-section of the flow at flood tide. Here the strong jet in the northern part of the channel is clearly visible, with speeds exceeding 5 m/s near the surface. From these figures it is clear that treating the flow through the passage as uniform – either in time or in space – is clearly inaccurate. Such variations in the flow will be significant in determining where turbines should be placed.

Fig. 2.11 shows a snap shot of the flow at flood tide for the high-resolution 2D simulation. It clearly shows the flood jet comes around Cape Split. It shows large eddies that are generated by the tip of Cape Split and then are advected along the passage, generating a recirculation zone along the split. Associated with these eddies is a pulse of strong flow that can extend across the jet. To the upper right of the figure, we can see a week eddy in West Bay that will be advected out into the passage as the tide turns as shown in the next figure.

Fig. 2.12 shows a snap shot of the flow just after the tide has turned from flood to ebb. It shows that at this time of supposed slack tide, the flow in the passage is dominated by large eddies. One off the tip of Cape Split generates strong flow along Cape Split. The other is the eddy from West Bay that has been advected into the passage, producing a small region of strong along the northern shore of the passage. This patch of strong flow is advected westward through the passage, leading to the pulse in high water speed before the ebb tide seen in both the observations and simulations, as illustrated in Fig. 2.4. Both these snap shots illustrate that as we increase the resolution of the numerical simulations, we will see more turbulent/unsteady flow features like eddies and waves. It is clear from Fig. 2.4 that such features will have a significant impact on the flow at a location and therefore the potential power generation at that location.

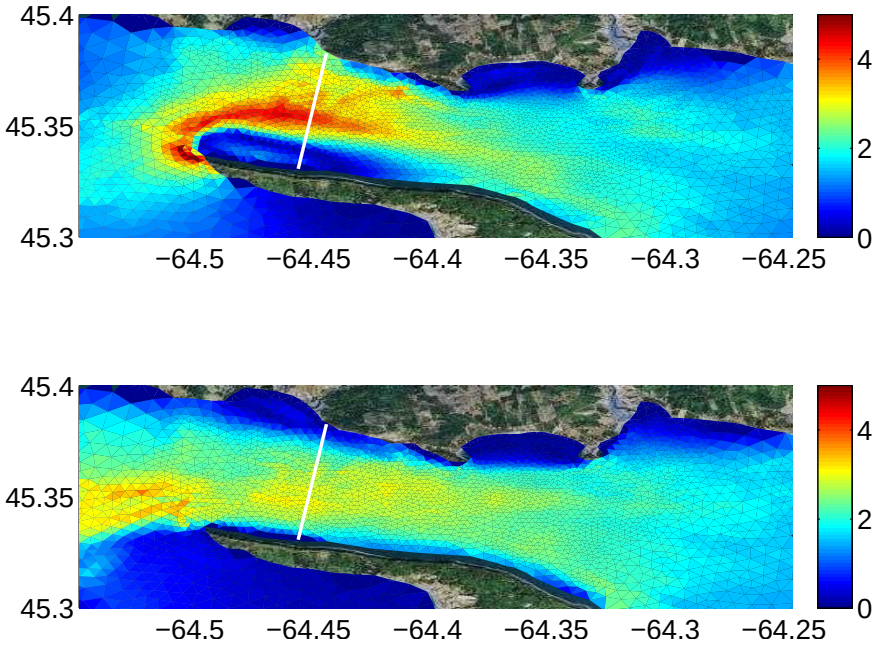

Figure 2.9: The depth-averaged speed through minas passage. at flood (top) and ebb (bottom) tides. Rhe white line shows the location of the cross-sections in Fig. 2.10 and the location of tidal fences. During flood tide the flow is left to right; during ebb tide it is right to left. Speeds are in metres per second.

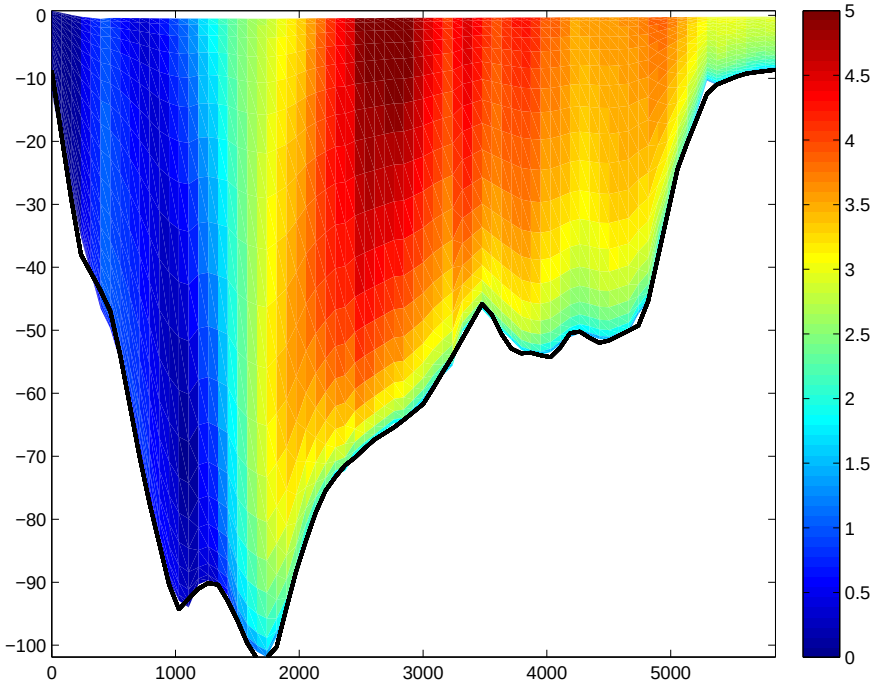

Figure 2.10: A cross-section of the flow speed through minas passage at flood tide. The location of the cross-section is shown in Fig. 2.9. The cross-section runs from the southern shore on the left to the northern shore on the right. speeds are in metres per second.

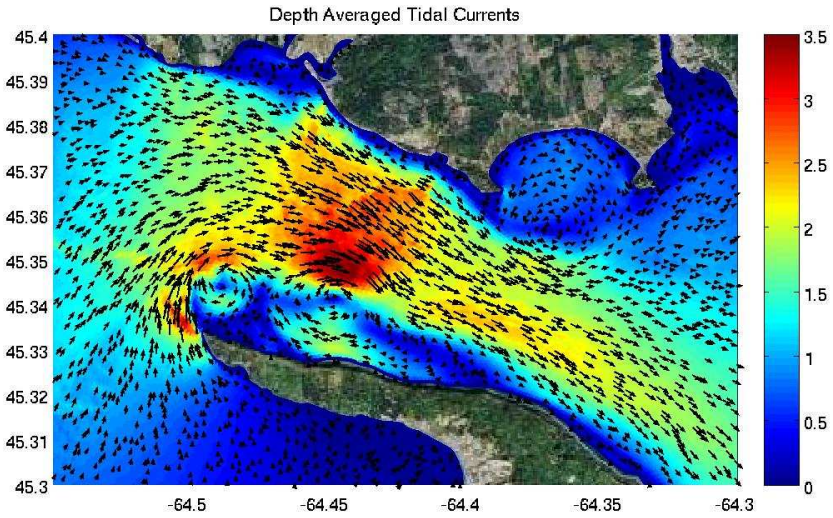

Figure 2.11: A snap shot of the flow through Minas Passage during flood tide from a high resolution 2D simulation. Note the eddies forming off the tip of Cape split and propagating through the channel.

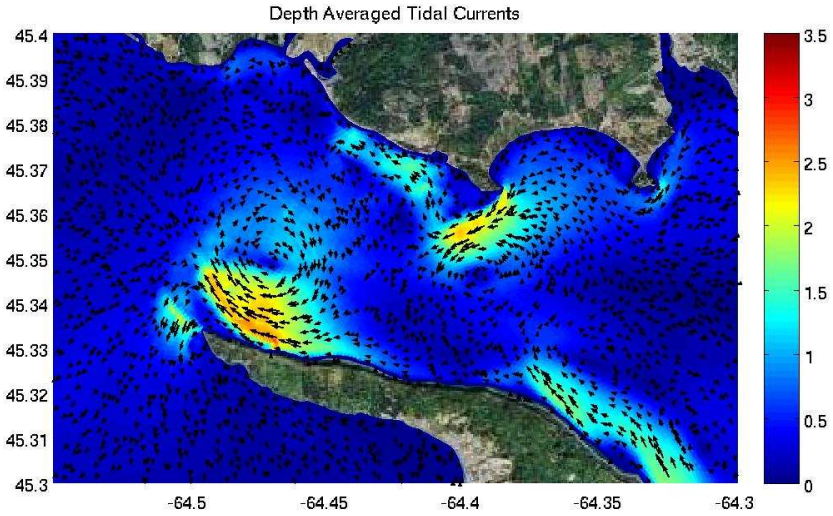

Figure 2.12: A snap shot of the flow through Minas Passage at the beginning of ebb tide from a high resolution 2D simulation. Note the large eddy off the tip of Cape Split and the eddy leaving West Bay that results in a pulse of high speed flow that is propagated through the FORCE test site.

2.2 Modelling power extraction from Minas Passage

The power potential of a fence of turbines in a channel can be estimated using LMADT. The theory uses momentum balances and Bernoulli equations to derive formulas for the flow past a turbine fence. Garrett and Cummins [15] illustrated how the Betz theory could be adapted to a finite channel, illustrating that since the channel restricts the flow, the potential power of a turbine fence changes as it occupies a larger portion of the channel cross-section. The theory assumed a small Froude number for the flow and ignored changes in water depth along the passage. Whelan et al. [16] illustrated how free surface effects and a finite Froude number could be included in the theory. Houlsby et al. [17] give a detailed derivation of the models, from the Betz formulation to the full LMADT. Finally, Draper et al. [18] present the LMADT theory and compare it to numerical simulations. Here, we give a brief review of the formulation of LMADT as presented in [15] and [18].

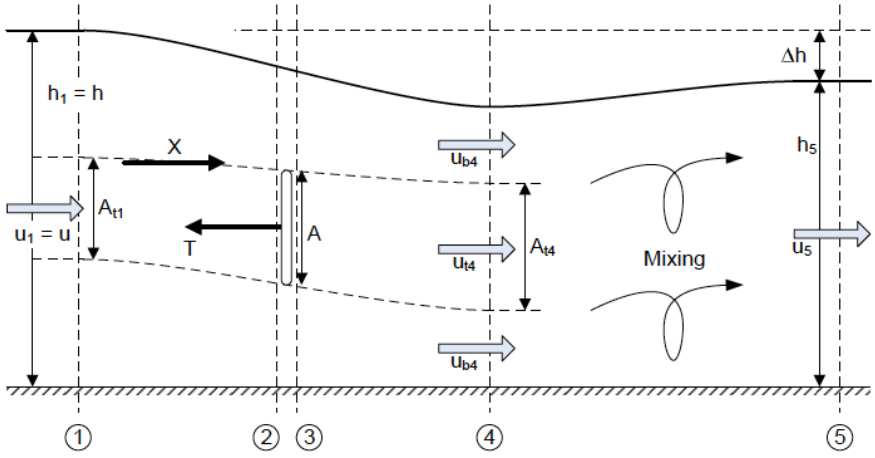

Figure 2.13: A figure describing the one-dimensional LMADT in an open channel flow. Taken from Draper et al. [18].

Fig. 2.13, taken from [18], gives the configuration of the flow past a partial turbine fence. The numbers along the bottom of the figure label the region of the domain: region 1 is far upstream from the turbine, region 2 is immediately upstream from the turbine, region 3 is immediately downstream from the turbine, region 4 is in the wake region downstream from the turbine, and, finally, region 5 is far downstream from the turbine, where the wake has mixed with the surrounding flow. The theory assumes the incoming flow, $u_1 = u$, is uniform with depth and across the channel.

Before we discuss the results of the full theory we begin with a quick review of Betz theory. This theory is well known in the engineering world as it gives a theoretical limit for the efficiency of an isolated turbine. It therefore gives a useful base for the discussion that follows. The theory considers the steady flow through and around an isolated turbine in an infinitely large and deep channel. That is, the situation shown in Fig. 2.13, but ignoring the

effects of the bottom, surface and sides of the channel. In doing so, the theory examines only the flow that passes through the turbine.

By considering the conservation of mass and momentum, and Bernoulli's equation, one can derive a equations that determine the dynamics of the flow. In the problem formulation, we have one remaining variable we can choose to describe how much energy the turbine takes from the flow. Mathematically, this is most easily done by setting the parameter

$$\alpha_4 = \frac{u_{t4}}{u}\,, \tag{2.2}$$

which is the ratio of the water speed in the turbine wake, u_{t4}, to the upstream water speed, u. Hence, varying α_4 is seen as tuning the turbine to extract more or less power from the flow.

The applying Betz theory, the flow through the turbine is then given by

$$u_{t2} = u\frac{1}{2}(1+\alpha_4). \tag{2.3}$$

and the turbine thrust is given by

$$T = C_T\left(\frac{1}{2}\rho A u^2\right) \tag{2.4}$$

where C_T is the thrust coefficient given by

$$C_T = 1-\alpha_4^2, \tag{2.5}$$

The power that the turbine generates can be found by multiplying the force on the turbine by the speed of the water flowing through the turbine, thus the power equation is simply

$$P = Tu_{2t} = C_P\left(\frac{1}{2}\rho A u^3)\right) \tag{2.6}$$

where

$$C_P = \frac{1}{2}(1+\alpha_4)(1-\alpha_4^2), \tag{2.7}$$

is the power coefficient and represents the fraction of the potential energy flux that is available to the turbine for electricity generation. It is easy to show that C_P has a maximum value of $16/27 = 0.59$ when $\alpha_4 = 1/3$. Indicating that a maximum of 59% of the kinetic flux power is available to generate electrical power when the flow speed through the turbine and in the wake are $2/3$ and $1/3$ the upstream speed, respectively. Actual turbines do not achieve such a high power coefficient. For example, the SeaGen two 16m diameter turbines are rated as producing 1.2 MW at a water speed of 2.4 m/s, which corresponds to $C_P = 0.42$.

An alternative formulation of writing the turbine thrust and power is to use a quadratic drag formulation written in terms of the flow through the turbine, u_{t2}, that is

$$T = C_D\left(\rho A u_{t2}^2\right), \quad P = C_D\left(\rho A u_{t2}^3\right), \tag{2.8}$$

where the turbine drag coefficient is given by

$$C_D = \frac{1}{2}\frac{1-\alpha_4^2}{\alpha_2^2}, \tag{2.9}$$

with $\alpha_2 = u_{t2}/u$. The maximum power occurs when $C_D = 1$.

Finally, we can use Betz theory to discuss the concept of the Power Extracted from the flow. In the above formulation, power is lost when the downstream flow mixes with the surrounding water. Therefore, the total power the turbine extracts from the flow is made up of two parts, power that is available for electricity generation and power lost in the wake. The power that is extracted from the flow is not all converted into useable energy. For this reason, we make a distinction between Power, P, and Extracted Power, P_{ext}. To distinguish between the two, Corten [19] gives the example of a boat towing a turbine through still water. The boat can be thought of as moving at a speed of u, while the flow through the turbine has a speed of u_{2t}. Clearly u_{2t} is going to be less than u. Also, the energy used to pull the turbine will not all be recovered by the turbine. P_{ext} can be thought of as the power used to pull the turbine, while P is the power that the turbine generates.

Since the turbine experiences the same thrust, but is travelling at speed u the power extracted is simply

$$\mathrm{P}_{ext} = Tu = C_T\left(\frac{1}{2}\rho A u^3)\right) \tag{2.10}$$

We can define the efficiency of the turbine as

$$\eta = \frac{P}{\mathrm{P}_{ext}} = \frac{C_P}{C_T} \tag{2.11}$$

Hence at maximum power, the power is 2/3 the extracted power. That is, only 2/3 of the power the turbine extracts from the flow is available for power generation, the other 1/3 is lost in the wake mixing process.

It is worthwhile to examine how the efficiency of the turbine changes if we change the design of the turbine, that is if we change C_D. In Fig. 2.14 we plot C_P and C_T versus the turbine drag C_D. It illustrates how the maximum power occurs at $C_D = 1$. It also illustrates that by decreasing the turbine drag, that is designing a turbine that takes less power from the flow, the efficiency can be increased. For example, with if we chose $C_D = 2/3$, ($\alpha_4 = 1/2$) we get $C_P = 9/16 = 0.5625$ and $C_T = 3/4$. That is the power only reduces from 59% to 56% of the KE flux, but the efficiency increases from 2/3 to 3/4.

In extending Betz theory to the LMADT as illustrated in Fig. 2.13, requires that we take into account the finite nature of the channel which the tidal current flows through. Most importantly, this introduces the concept of the blockage ratio,

$$B = \frac{A}{A_C}\,, \tag{2.12}$$

which is the ratio of the turbine fence cross-sectional area, A, to the cross-sectional area of the channel, A_C, and thus is the portion of the channel cross-section occupied by turbines. In

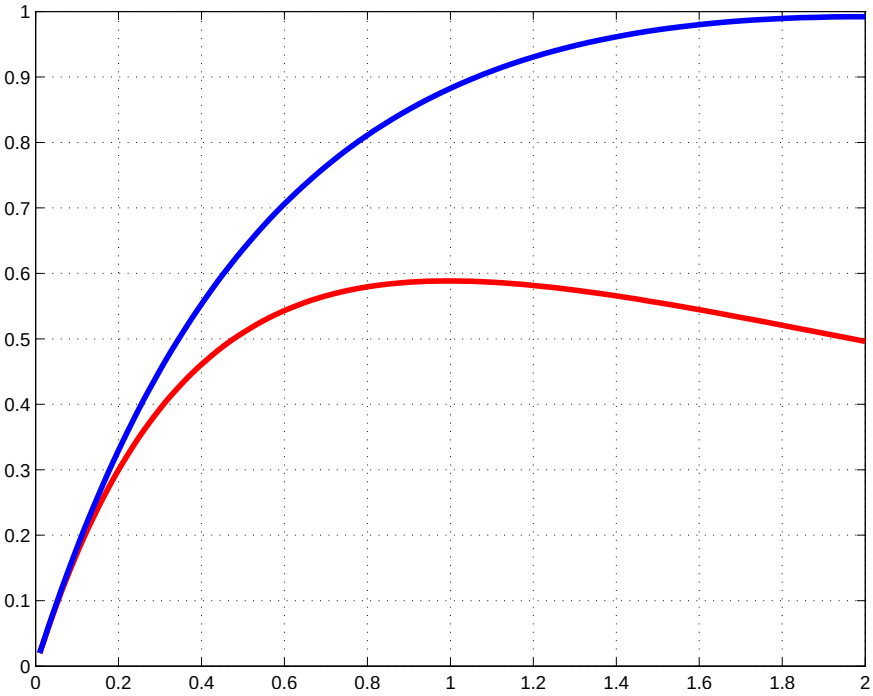

Figure 2.14: The power coefficient C_P (blue) and the thrust coefficient C_T (red) versus the relative flow speed in the wake, C_D for Betz Theory. The two curves show the relationship between the power available for generation (blue) and the power extracted from the flow (red).

Betz theory, $B = 0$, in the full fence theory of [4], $B = 1$. We must also consider how the free surface affects the dynamics. This is represented in the theory through the Froude number, $Fr = u/\sqrt{gh}$, which is set by the depth of the water in the channel and the upstream flow speed. The full details of the theory are somewhat complex, see [20, 18, 17, 15]. In the new formulation, we must also consider the flow around the turbine, in particular the flow outside the wake with speed u_{b4}.

Following [18], we can calculate $\beta_4 = u_{b4}/u$ by finding the solution of the quartic equation

$$\frac{Fr^2}{2}\beta_4^4 + (2\alpha_4 Fr^2)\beta_4^3 - (2 - 2B + Fr^2)\beta_4^2$$

$$-(4\alpha_4 + 2\alpha_4 Fr^2 - 4)\beta_4 + \frac{Fr^2}{2} + 4\alpha_4 - 2B\alpha_4^2 - 2 = 0 \tag{2.13}$$

and, thus, obtain the speed of the flow outside the turbine wake, u_{b4}. Here, Fr is the Froude number defined by $Fr = u/\sqrt{gh}$, which we will calculate based on the undisturbed flow speed. When the Froude number is set to zero, Equation 2.13 reduces to a quadratic equation in β_4 that is equivalent to equation (2.22) in [15]. After finding β_4, we can calculate the flow through the turbine, u_{2t}, by calculating $\alpha_2 = u_{2t}/u$ using the formula

$$\alpha_2 = \frac{\alpha_4(\beta_4 - 1)}{B(\beta_4 - \alpha_4)}\left(1 - \frac{Fr^2}{2}\beta_4(\beta_4 + 1)\right). \tag{2.14}$$

It should be noted that a physically acceptable solution to Equations 2.13–2.14, that is, β_4 is a real number with $\beta_4 \geq 1$ and $0 \leq \alpha_2 \leq 1$, is not possibile for all values of B, Fr, and α_4. (see [18] for more details). Fortunately, this is not an issue for the small blockage ratios discussed in this paper.

Following the theory (see [20, 18, 17, 15])

Having calculated the flow, we can calculate the turbine thrust. Here, we choose to write the thrust as a quadratic drag

$$T = C_D \rho A (u_{2t})^2, \tag{2.15}$$

where the turbine drag coefficient is given by

$$C_D = \frac{1}{2}\left(\frac{\beta_4^2 - \alpha_4^2}{\alpha_2^2}\right). \tag{2.16}$$

Thus, using LMADT, we can calculate the drag coefficients of the turbine fence knowing only B and α_4. Specifying the flow in the wake of the turbine is an odd way to describe the design of a turbine. Here, we choose to present our results in terms of the turbine drag coefficient, C_D. Alternatively, one could specify the reduction of flow through the turbine, α_2, or the axial induction factor, $1 - \alpha_2$.

We can also write the turbine thrust as an effective quadratic drag on the upstream flow through the entire channel cross-section; that is, we write

$$T = C_{D_F} \rho A_c u^2, \tag{2.17}$$

where the effective fence drag coefficient is given by

$$C_{D_F} = \frac{B}{2}(\beta_4^2 - \alpha_4^2)\,. \tag{2.18}$$

Finally, we can calculate the turbine power,

$$P = Tu_{2t} = C_P \frac{1}{2}\rho A u^3\,, \tag{2.19}$$

with the power coefficient given by

$$C_P = \alpha_2(\beta_4^2 - \alpha_4^2)\,, \tag{2.20}$$

and the total power extracted from the flow,

$$P_{ext} = Tu = C_{D_F}\rho A_c u^3\,. \tag{2.21}$$

As discussed in [15], the difference between the turbine power, P, and the total extracted power, P_{ext}, is the power lost in the merging of the turbine wake and the free stream. The details of power lost in the wake are discussed in more detail in [17, 18].

While LMADT calculates the power of a turbine fence, it does not determine u, the speed of the flow through the channel. As the calculation in KMLH illustrates, calculating this flow is essential in determining the power potential of a channel and the impact that power extraction will have on the flow through the channel. Recently, Vennell [21] illustrated that the LMADT as presented in [15] could be combined with the theory of turbine impact on the flow through the channel as presented in[5] to determine the power potential of a partial turbine fence in a given tidal flow. His analysis illustrated a couple of key points. First, turbines can be tuned by changing their drag coefficient to maximize the power generated for a specific arrangement of turbine fences in a given channel. Second, the maximum potential power of a channel can be realized with partial fences by adding sufficient rows of these fences to the channel.

The theory in KMLH calculates the volume flux through Minas Passage as a function of a non-dimensional drag coefficient,

$$\lambda_T = \frac{C_{D_F}}{C_{D_0}}\,, \tag{2.22}$$

where C_{D_F} is the effective fence drag coefficient given by Equation 2.18 and C_{D_0} is the natural drag coefficient of the passage; that is, C_{D_0} is the drag coefficient of momentum lost through bottom drag and nonlinear inertia. Therefore, λ_T represents the ratio of the turbine drag to the natural drag in the system. From the analysis in KMLH, we can estimate that $C_{D_0} = 1.8$.

Following KMLH, the flux through the passage with turbines is

$$Q(\lambda_T) = R(\lambda_T)Q_0\,, \tag{2.23}$$

where Q_0 is the undisturbed peak flux through the passage here estimated from our numerical simulations to be 8.4×10^5 m^{3}s^{-1}. The reduction in flow factor, R, is given by

$$R(\lambda_T) = \left(\frac{1 + \sqrt{1+\delta}}{1 + \sqrt{1 + \delta(1+\lambda_T)^2}} \right)^{1/2} . \tag{2.24}$$

The parameter δ in the formula is determined by the geometry of the system and the natural drag in the basin. It can be written in terms of the nondimensional parameters given in KMLH as follows:

$$\delta = \frac{4(\lambda_0^*)^2}{(\beta - 1)^4} . \tag{2.25}$$

Using the values for these parameters for Minas Passage as given in KMLH—$\beta = 7.6$, $\lambda_0^* = 9.9$—gives $\delta = 0.2$. Therefore, given the effective fence drag coefficient C_{D_F}, one can calculate the flux through the passage and, hence, the water speed in the passage given by

$$u = \frac{Q}{A_c} . \tag{2.26}$$

Finally, the calculation of the turbine power given by Equation 2.19 must be adapted to reflect that the tidal flow varies with time; that is, water speed is

$$U = u \cos \omega t ,$$

where for simplicity we will assume a single tidal constituent with frequency ω, a reasonable assumption for the M_2-dominated tides in the Bay of Fundy. Then the mean turbine power is

$$P_{avg} = \overline{C_P \frac{1}{2} \rho A (u|\cos(\omega t)|)^3} = C_P \frac{1}{2} \rho A u^3 \left(\frac{4}{3\pi} \right) , \tag{2.27}$$

where the factor of $4/3\pi \approx 0.42$ just reflects the reduction in power associated with the water speed oscillating from 0 to its maximum u. That is, the mean power is roughly 42% of the maximum power during the tidal cycle.

To summarize, given a chosen blockage ratio B and wake speed ratio α_4, we can use LMADT to calculate the effective turbine-fence drag using Equation 2.18 with Equations 2.13–2.14. We can then use this drag to calculate the new volume flux through the passage using Equations 2.23–2.25 and the water speed in the passage using Equation 2.26. Finally, we calculate the turbine power using Equation 2.27. Thus, we can estimate the power potential of a given turbine fence and the reduction in flow through the passage.

It should be noted that for an isolated turbine, $B \ll 1$, the theory reduces to the Betz limit with a maximum power at $\alpha_2 = 2/3$, $\alpha_4 = 1/3$, and $\beta_4 = 1$ giving $C_P = 0.59$, $C_D = 1$. For a complete turbine fence, $B = 1$, the results of KMLH are recovered if one assumes the Froude number to be zero.

For simplicity, we first consider the case where $Fr = 0$ as it allows for figures that are easier to slightly interpret. We first look at the properties of maximum power for each value

of the blockage ratio. Fig. 2.15 illustrates how the properties of the maximum power change versus blockage ratio, B. In Fig. 2.15 A) the turbine drag that gives maximum power is plotted. It shows that as a fence occupies a greater portion of the cross-section, the turbine drag can be increased from the isolated turbine value of 1 to values greater than 20. This is not surprising because the turbine used in a tidal barrage would be of substantially different design than a stand alone turbine. Increasing the turbine drag for larger fences substantially increases the power they can generate.

The increase in power is shown in Fig. 2.15 B). Here we plot the maximum power normalized by the undisturbed kinetic energy flux through the turbine region, that is, P/P_{KE}, where

$$P_{KE} = \frac{1}{2}\rho A\overline{u^3}\,.$$

(Note this is not identical to C_P.) For small B, LB theory applies and the maximum power is 59% of the kinetic energy flux. However, as we increase B the maximum power increases more rapidly than the simple increase in turbine area, and for large fences the maximum power can be more than five times the kinetic energy flux. As discussed in KMLH, this results from the fact that the turbines increase the tidal head across the passage by increasing the phase lag of the tides. The larger tidal head creates a larger hydrostatic pressure force across the channel, which can force water through turbines with much higher drag coefficients leading to greater power. Again, this is because a large fence of turbines acts much like a barrage, taking advantage of the power in the potential energy in a large tidal head.

In Fig. 2.15 C) we examine the efficiency of the turbine fence, here defined as the ratio of maximum power, P_{max}, to the total power extracted, P_{ext}. Again for small B, LB theory applies and the efficiency is 2/3; that is, 2/3 of the power extracted from the flow is due to the drag of the turbine. As B increases, the efficiency initially decreases. This is important since most turbine arrays are likely to be in the region of moderate values of B. When $B > 0.5$, the efficiency increases eventually, reaching 1 at $B = 1$, where no power is lost because all the flow passes through the turbines. It should be noted that one can improve the efficiency for any value of B by decreasing the drag, with, of course, a reduction in the turbine power.

Finally, in Fig. 2.15 D) we examine the reduction in the flow through the passage caused by the turbines. Any reduction in the flow through Minas Passage will lower the tides in Minas Basin and could have important effects on the ecology of the region. To examine the impact of the turbines, for each value of B we assume the turbines are designed to generate maximum power (that is, the drag value in plot A). We then plot the power per percent change in flow versus B. The value decreases from 570 MW to 220 MW as B increases from 0 to 1. This suggests that isolated turbines generate power with the least impact on the flow through the passage. However, it should be noted that this is for turbines producing maximum power. If we reduce the drag of these turbines, we can increase this value. Interestingly, in the limit as C_D goes to zero, we get 870 MW for a one percent change in flux for all B. This is close to the value of 770 MW calculated in KMLH for a full fence.

We can also examine the relationship between turbine power and impact on the flow. In Figs. 2.16 , we plot the turbine power versus blockage ratio B and wake speed α_4 for Minas

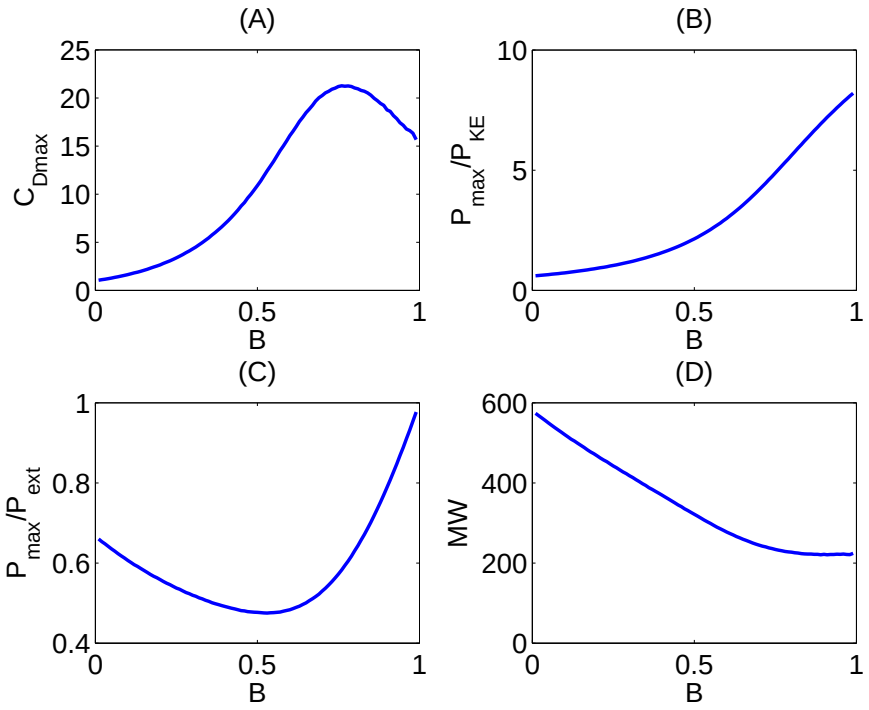

Figure 2.15: A) The value of the drag, C_D, that produces the maximum turbine power versus B. B) The ratio of the maximum power to the undisturbed kinetic energy flux versus B. C) The efficiency of the turbine fence, P/P_{ext} at maximum power versus B. D) The power per percent change in flow at maximum power versus B.

Passage with $Fr = 0$. The figures show how the maximum power increases dramatically with increasing blockage ratio, and reaches the nearly 8 GW value seen in [4]. It should also be noted that the maximum power incurs at increasingly large α_4 as the blockage ratio increases. In Fig. 2.16, we also plot the amount of turbine power in MW per percentage reduction in the flow through the channel versus blockage ratio B and wake speed α_4 for Minas Passage with $Fr = 0$. This is another measure of efficiency, we would like to produce power while having the least impact on the environment. Therefore, as before we get a trade off between power and impact.

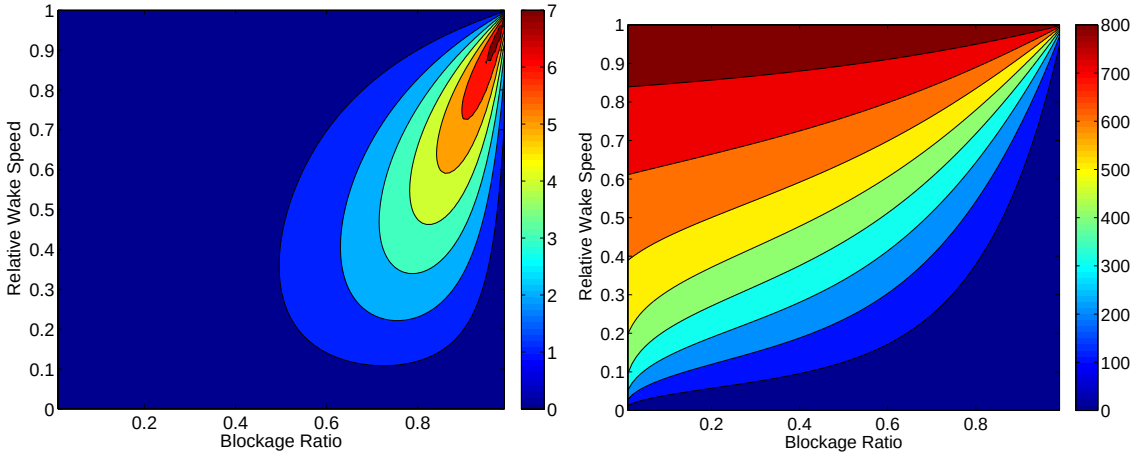

Figure 2.16: (Left) The turbine power in GW versus blockage ratio B and wake speed α_4 for the Minas Passage with $Fr = 0$. (Right) Turbine power per percentage change in the flux through the channel.

Here, we are concerned with realistic arrays of in-stream turbines deployed on the sea bed. The average depth of Minas Passage is about 50 m. If we assume the turbines have a height of 20 m, then we have that $B < 0.4$. Therefore, we restrict our analysis to relatively small values of B. However, we expect that many rows of turbine fences with small blockage ratios will be deployed. Following [21], we can model N_R rows of turbine fences by simply aggregating their effect. That is, we replace the formula for the effective fence drag coefficient given by Equation 2.18 with

$$C_{D_F} = N_R \frac{B}{2}(\beta_4^2 - \alpha_4^2)\,, \tag{2.28}$$

and the mean turbine power Equation 2.27 becomes

$$P_{avg} = N_R C_p \frac{1}{2}\rho A u^3 \left(\frac{4}{3\pi}\right)\,. \tag{2.29}$$

In order to illustrate the results of the theory we choose four blockage ratios—0.4, 0.2, 0.1, and 0.05—which roughly correspond to fences of 310, 155, 77 and 38 turbines with cross-sectional area 400 m^2 across Minas Passage. In Figs. 2.17 and 2.17, we plot the mean

turbine power and the resulting reduction in flow through the passage versus the turbine drag coefficient. For these plots, the total turbine area is set to twice the total cross-sectional area of the passage. That is, the results are for 5 rows at a blockage ratio of 0.4, 10 rows at 0.2, 20 rows at 0.1, and 40 rows at 0.05. In total, they correspond to arrays of roughly 1550 turbines.

The first conclusion we can draw is that such arrays of turbines can generate 1500 to 2500 MW of power with only a 3 to 5% reduction in the flow through the passage. That is, the change from a full barrage of turbines to rows of partial fences has not drastically changed the conclusions of KMLH. The next conclusion we can infer is that a higher blockage ratio results in greater power. The greater power occurs for two reasons. First, at an equal drag, a higher blockage ratio results in a higher flow through the turbine—a larger value of α_2—and, thus, the power is greater. Second, the drag can be increased to higher values when the blockage ratio is higher. While the maximum power occurs when the drag is 1 for small blockage ratio, corresponding to the Betz limit, the maximum power occurs at a drag of 4 for $B = 0.4$. For small values of drag, all the fences give similar results.

Comparing Fig. 2.17, we see that the reduction in flow increases with increasing power, as one would expect. We can also conclude that tuning the turbines to reach maximum power can be costly in terms of their impact. For example, with $B = 0.4$, 2500 MW of power results in less than a 4% reduction in flow, while increasing this to 3300 MW of power results in an over 8.5% reduction in flow. Generating the extra 800 MW has a very large impact on the flow. One can conclude that it may be better not to increase the turbine drag to large values beyond $C_D = 1$. It is worth noting that when $C_D = 1$, the effective fence drag coefficient C_{D_F} varies from 0.95 for $B = 0.05$ to 1.3 for $B = 0.4$. Thus in all these cases, $C_{D_F} < C_{D_0}$, the effective drag of some 1500 turbines is less than the natural drag in the passage!

In Fig. 2.18 we plot results where we hold the turbine drag constant, $C_D = 1$, and vary the number of rows of turbines. We see that the power increases almost linearly for small blockage ratios, with each turbine producing roughly 1 MW. Increasing the blockage ratio to 0.4 increases the power by almost 50%, with each turbine producing over 1.5 MW. The power per turbine does decrease, albeit slowly, as the increased number of turbines begins to decrease the speed through passage.

On the right in Fig. 2.18 we plot the turbine power versus the reduction in flow for the cases shown on the left. The four curves here are remarkably similar, implying that the different blockage ratios and number of fences do not drastically change the relationship between the power generated and the impact on the flow. For example, for a 5% reduction in flow, the power ranges from 2600 to 3000 MW. For small amounts of power (< 1500 MW), we can generate approximately 750 MW of turbine power for each percent of flow reduction, in agreement with KMLH. This power rate is reduced as the number of turbines increases, down to only about 500 MW when the power exceeds 3500 MW. Note that in these figures, we have limited the power to only 4000 MW. One can continue to increase the number of rows until the power reaches the theoretical maximum of near 8000 MW, but this would occur at an unrealistically high number of rows and an unacceptably high reduction in the

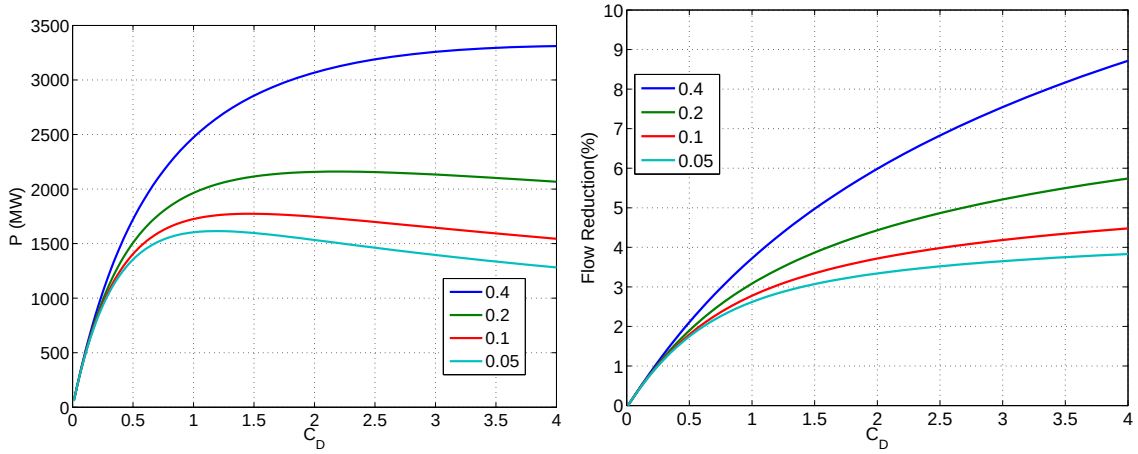

Figure 2.17: (Left) The total turbine power (MW) versus the turbine drag coefficient for four different blockage ratios. For each blockage ratio, the number of rows of turbines is chosen so that the total cross-sectional area is equivalent for all cases. (Right) The reduction in flow through the passage versus the turbine drag coefficient for the four different blockage ratios shown on the left.

flow through the passage.

In summary, the adaptation of LMADT theory presented here allows for several simple conclusions. First, 2000 to 2500 MW of theoretical turbine power can be realized for less than a 5% reduction in flow through the passage. Second, if the blockage ratio is increased, it will result in greater power per turbine, even if we do not tune the turbines to have a higher drag. Third, if the turbines are tuned to increase the turbine power, it comes at the cost of a much higher reduction in flow. Finally, the relationship between turbine power and reduction in flow does not depend strongly on the blockage ratio.

2.3 Numerically simulating power extraction from Minas Passage

The results of our numerical simulations can be used estimate potential power generation given a power curve for a specific turbine. To illustrate this we constructed a typical power curve for a 400 m^2 turbine rated for 1.2 MW at 2.4 m/s, as shown in left plot in Fig. 2.19. We also estimated the total power extracted from the flow, by using Betz theory and a rough approximation of the structural area (1/5 of the turbine) and the structural drag coefficient, 0.2. Note that the power extracted decreases as the turbine regulates the power generated. We have assumed that the turbine will regulate the power generated by some mechanism like changing the pitch of its blades, will reduce the drag of the turbine. As shown in Fig. 2.14, this increases the efficiency of the turbine. This increase in efficiency is exceeded by the drag on the supporting structure as the water speed increases. In the right plot in Fig. 2.19,

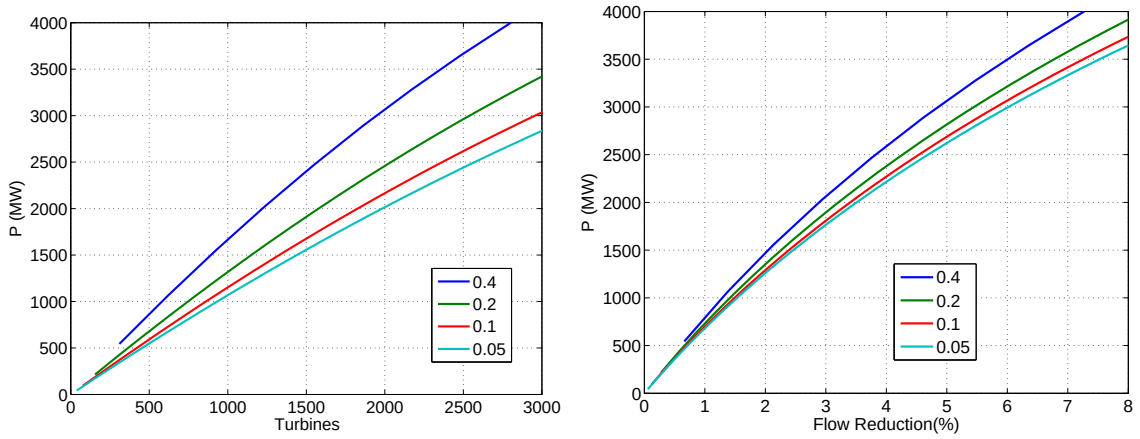

Figure 2.18: (Left) The total turbine power (MW) versus the number of turbines for four different blockage ratios. The turbine drag coefficient is held constant, $C_D = 1$, and the number of turbines is increased by increasing the number of rows of turbines. Each turbine is assumed to have a cross- sectional area of 400 m^2. (Right) The total turbine power (MW) versus the reduction in flow through the passage for four different blockage ratios, as shown in Fig.2.18. As the number of turbines increases, one moves from left to right along the curves.

we show how a time series of water speed can be converted to a time series of power and extracted power. For this location, the 1.2 MW turbine generates a mean power of 0.7 MW while extracting 1.7 MW of power from the flow, an efficiency of about 40%.

In figure Fig 2.20, we use a month-long time series of water speed from a high resolution 2D simulation of the flow through Minas Passage and the power curve in Fig. 2.19 to calculate the mean power generation at each location. The figure shows that there is a large portion of Minas Passage where the flow speed is sufficient to have this turbine generate significant power, like that shown in Fig. 2.19. Most of this region is in the northern section of Minas Passage, where the flood jet is strong and away from the recirculation zone along Cape Split (see Fig. 2.11) Much of the high energy region lies in water that is deeper than 50 m, and the majority of it lies in between 50 and 70 m.

In order to model turbines in the 3D numerical simulations model, we used the simple approach of adding a quadratic drag term to the horizontal momentum equations i.e., the u-momentum equation would have the additional forcing term

$$-\frac{C_D}{W} u \sqrt{u^2 + v^2}\,, \tag{2.30}$$

where u and v are the north-south and east-west velocities, respectively;C_D is the drag coefficient of the turbines; and W is the thickness of the turbines along the direction of flow. This is the most natural extension of the work in KMLH and is easy to employ in a finite-element model where we wish to change the locations of the turbines without altering the numerical grid. The major disadvantage of this approach is that it represents relatively thin

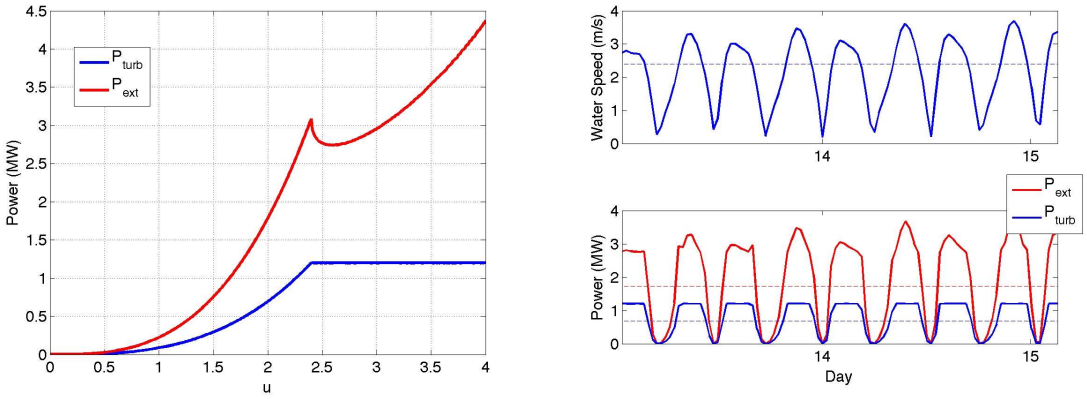

Figure 2.19: Right: In blue, the power curve for a turbine that is rated for 1.2 MW at 2.4m/s. In red, an estimate of the power extracted by such a turbine. Left: A time series of water speed on Top and, bottom, the resulting power (blue) and extracted power (red). Over a year, the turbine generates a mean power of 0.7 MW and extracts 1.7 MW of power for a 40% efficiency.

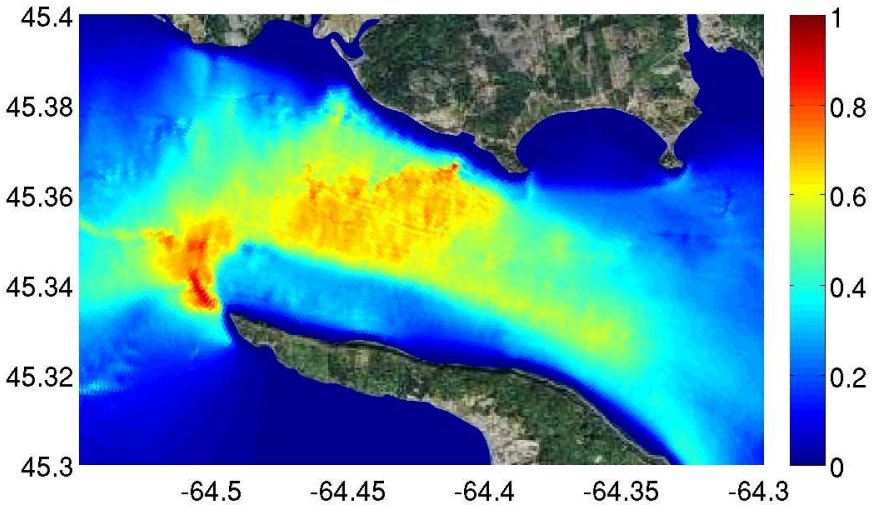

Figure 2.20: A plot of the estimated power generation at each location using the water speed data from a numerical simulation and the power curve shown in Fig. 2.19. The power the mean power generated over a full tidal cycle and is given in MW.

turbines with a large region of high drag. In fact, due to the grid resolution, the thickness of the turbine region is usually several hundred metres. One could raise many other issues with this model of turbines, but it serves the purpose of allowing us to extract power from the flow anywhere in the numerical grid.

After a simulation has been completed, the power extracted by the drag can be calculated as

$$P(t) = \rho \int \frac{C_D}{W} \left(u^2 + v^2\right)^{3/2} dV \,. \tag{2.31}$$

The mean power, P_{avg}, is simply this power averaged over a tidal cycle.

It is worth noting the effect of such a turbine barrage on the flow through the passage. In contrast to the flow shown in Fig. 2.10, the flow through the turbine region is almost completely homogeneous throughout the channel cross-section, both at flood and ebb tides. Thus, it is not too surprising that the 3D model replicates the 2D results since the turbine barrage eliminates all vertical variations in the flow. The vertical shear in the flow returns downstream from the turbine.

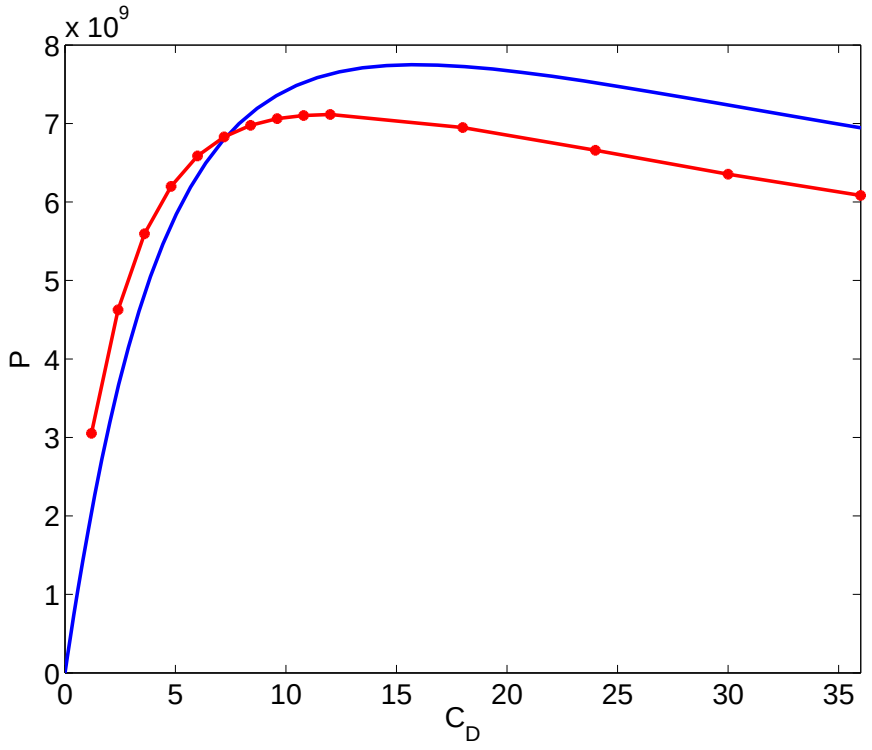

Figure 2.21: Turbine power, P, for a full fence versus the turbine drag, C_D. The blue curve is the theory and the red curve represents the numerical simulations (each dot represents an individual simulation).

In order to test the theories of Section 3, we ran numerical simulations with several turbine fences using the full 3D model described previously. We chose fences of turbines

across the cross-section shown in Fig. 2.10, whose location is shown in Fig. 2.9. Most fences were 600 m thick; one set of simulations was run with a fence only 300 m thick. For partial fences, we chose a line of 20-m-high turbines placed either at the surface or along the bottom. These were chosen to model the two most popular forms of turbines being examined. As well, these were chosen to emphasize the impact of turbine location in the water column, as Fig. 2.10 clearly shows the significant difference in speed between the surface and bottom flows. The turbines were only placed in water that was at least 40 m deep, giving $B = 0.21$.

In Fig. 2.22, we plot the turbine power versus the turbine drag for the three cases: surface turbines of thickness 600 m, bottom turbines of thickness 600 m, and bottom turbines of thickness 300 m. We also plot the curve from the theory with $B = 0.21$. First, it is clear that the theory and the simulations do not agree well. While the theory suggests the fence should have a maximum power of 190 MW at a drag of 2.8, the numerical simulations give maximum powers of 1090 MW and 720 MW at drags of 7.2 and 20 for the surface and bottom turbines, respectively. The simulations of bottom turbines with a thickness of only 300 m were run to see if the thickness of the simulated turbines could account for this discrepancy. Reducing the thickness reduces the maximum power to 562 MW at a drag of 18. However, this is about the minimum thickness that the grid resolution will allow. The small reduction in power suggests that the turbine thickness is not the only factor in the discrepancy. In fact, it may only reflect that at a thickness of 300 m the fence has become almost too thin for the grid resolution.

It should be noted that the surface turbines generate more power, as one would expect given the faster flow at the surface, as seen in Fig. 2.10. However, the difference is not as large as one might expect, leading to the conclusion that turbines deployed at the bottom of Minas Passage can still extract significant power from the flow.

In order to shed further light on how the simulated turbines alter the flow, we examined the changes in velocities that they produced. In Fig. 2.23, we plot a cross-section of the mean water speed from a simulation with bottom turbines producing maximum power. The speed is plotted as the relative change from the undisturbed speed; that is, a value of 50% would mean the mean water speed was reduced to half its original value and a value of 150% would mean it was increased to 1.5 time its original value. The location of the turbine fence is clearly indicated by the region of reduced water speeds at the bottom. The water speeds through the turbines are reduced to between 30% and 40% of their original values. This is significantly less than the theoretical value of 55%.

As well, it should be noted that the water speeds above the turbine increase significantly, by as much as 150%. The largest change is seen in the southern part of the cross-section, as the flood jet seen in Fig. 2.10 has been strengthened, widened, and shifted southward. A similar change in speeds is seen for the surface turbines, though of course the decrease is now at the surface and the increase at the bottom. These large increases in flow need to be considered carefully when installing turbine fences.

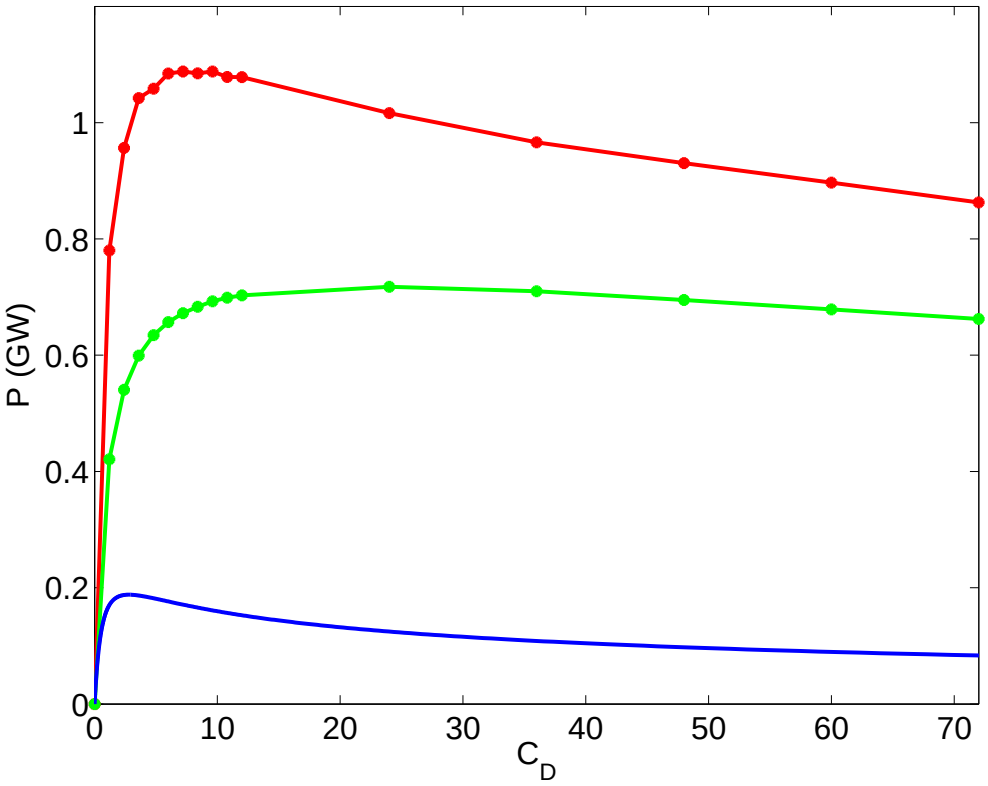

Figure 2.22: Turbine power for a partial fences versus the turbine drag, C_D. The blue dashed curve is the theory, the red, green, and black curves are the numerical simulations of surface, bottom, and half-thickness bottom turbines, respectively (dots represent each simulation.)

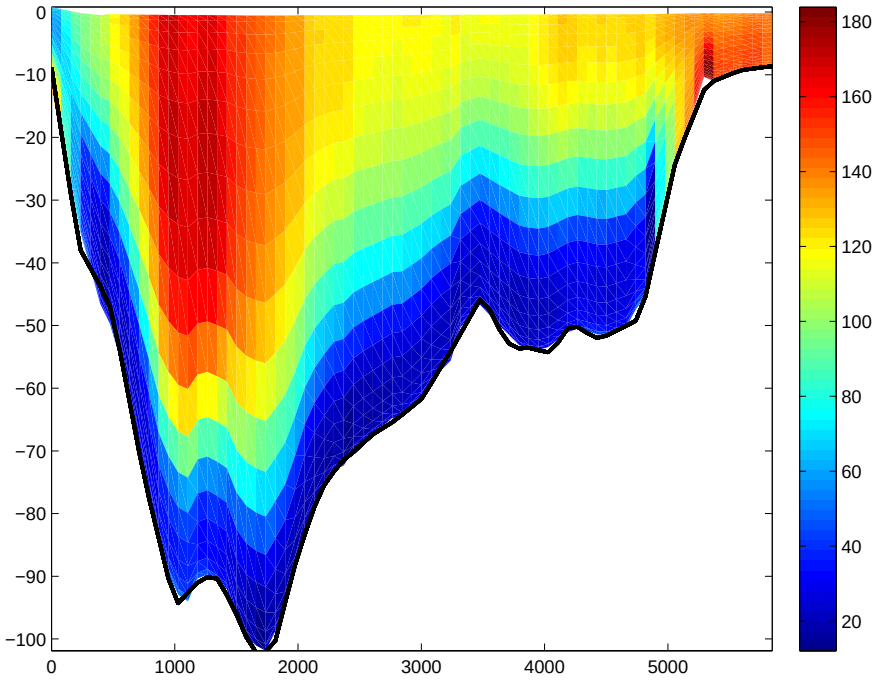

Figure 2.23: The new water speed relative to the undisturbed water speed as a percentage.

2.4 Turbine Array Analysis for Minas Passage

The above analysis presents interesting conclusions in terms of the potential power and impact of a series of turbine fences. However, it does not address where the turbines should be placed in the passage or whether there is sufficient space in the passage to locate the thousands of turbines. In spacing the turbines, we must consider the size of the turbine wakes. As well, in order to assess the power potential of an actual turbine array, we need to consider the spatial variations in potential power illustrated in Fig. **??**. In this section, we take these factors into account to produce a model that uses water speeds from numerical simulations to predict the power and impact of realistic turbine arrays.

To start, we take the depth-averaged speed from our numerical simulation and interpolate from the finite-volume grid onto a regular 20 m by 20 m grid in a coordinate system with x running along the passage and y running across the channel with $y = 0$ marking the centre of the channel. The result is shown in Fig. 2.24. A turbine can be placed in any of the grid boxes, resulting in over 100,000 possible turbine locations. As well, for each turbine array we can specify the turbine drag, allowing for the possibility of tuning the array.

For each turbine array, we calculate the turbine power and new flow through the passage as follows. First, the channel is divided into cross-channel strips that are 10 turbine diameters in length. For each strip, we apply LMADT to calculate the turbine flow factor, α_2; the effective fence drag coefficient, C_{D_F}; and the power coefficient, C_P. Then, to apply the theory of KMLH we calculate the total turbine drag coefficient of the channel, λ_T, as a

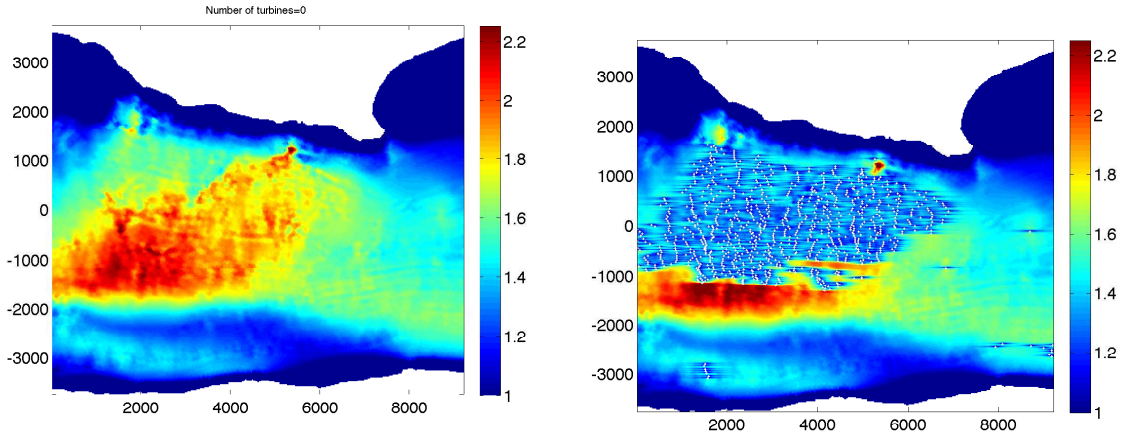

Figure 2.24: (Left)The flow speed from a numerical simulation interpolated onto a regular 20 m by 20 m grid. The flow speed is the depth- and time- averaged speed given in metres per second. The values for the x and y coordinates are in metres. The white region is land. (Right) The flow speed after 1000 turbines have been added. The strips of lower flow shown in blue are the wakes of the turbines. They are roughly 400 m long, extending 200 m or 10 turbine diameters on either side of the turbine. In the wake the flow is reduced to roughly 2/3 the original flow.

weighted sum of the effective drag coefficients—in the sum the coefficients are weighted by the cross-sectional area of each strip. We use this to calculate the reduction in the flux through the passage, $R(\lambda_T)$, using Equation 2.24.

Next, we approximate the wake of each turbine. The details of a turbine wake can be difficult to determine and will depend on the specific design of the turbine. We know there will be a reduction in the water speed in the wake, and the turbulent flow will mix with the surrounding fluid as we move farther downstream from the turbine. Therefore, we assume that the wake decays exponentially from the turbine with length scale w_x times the turbine diameter, T_d, taken to be 20 m. Finally, since the wake cross-sectional area must be larger than the turbine area, we also assume the wake has a cross-channel length scale of w_y times the turbine diameter. From these considerations the water speed in the wake, $u_w(x, y)$, of a turbine located at (x_0, y_0) is

$$\frac{u_w}{u} = 1 - \frac{1+\alpha_4}{2} \exp\left(- \left(\frac{|x - x_0|}{w T_d} + \left(\frac{y - y_0}{T_d} \right)^2 \right) \right) , \tag{2.32}$$

where u is the undisturbed speed. Note that the factor $(1 + \alpha_4)/2$ accounts for the fact that, in tidal flow, the point (x, y) is upstream from the turbines half of the time and in the turbine wake the other half of the time. So, for example, in the Betz limit when $\alpha_4 = 1/3$, the flow is reduced to 1/3 its original value in the wake, so on average over an entire tidal cycle the flow is reduced to 2/3. Admittedly this is a crude representation of a turbine wake,

but it gives a rough idea of how the turbines must be spaced. At the turbine location itself, the flow is reduced by the factor α_2.

After calculating the wake speed and the flow through the turbines, we recalculate the mean velocity on each cross-section so that it has the new flux as stipulated by the reduction factor, $R(\lambda_T)$. This step will increase the speed of the flow around the turbines; that is, it is similar to the calculation of β_4 in LMADT. But now, the calculation also includes the effect of the turbine wakes. In the end, the result is the calculation of a new speed at every grid location. This new speed accounts for the impact of LMADT, the reduction in flow through the passage, and turbine wakes. An example of the resulting flow field around 100 turbines is shown in Fig. 2.24 in the right figure. The reduction in flow in the turbine wakes is clearly visible.

The mean turbine power can then be calculated for each turbine:

$$P_{avg} = C_P \frac{1}{2} \rho A \overline{u}^3 \left(\frac{\pi^2}{6} \right) , \tag{2.33}$$

where the constant factor in Equation 2.33 has changed because the speed is now the mean speed and not the maximum speed. It should be noted that this power will vary for every turbine since every location has a different speed. The total power is simply a sum of the powers of all turbines.

The final aspect of assessing turbine arrays is determining how to choose the location of the turbines. We are interested in arrays that maximize power. However, finding the optimal location of thousands of turbines given the 100,000 possible locations is an extremely difficult, if not impossible, problem. Instead, we take a simple sequential approach. We place the first turbine at the location with the highest speed. We then use the model to calculate the new speed. We use this new speed to place the second turbine, and so on. The result is a near-optimal placement of the turbines. Using this process, the turbines tend to align themselves into fences as shown in Fig. 2.24.

The focus of the results here is not the particular location of the turbines, since the actual position of turbines will require detailed knowledge of the turbines, the tidal currents, the sea bottom, the connecting cables, etc. Instead we examine only one aspect of the turbine positioning, restricting the depth of water where turbines can be deployed. Currently, most developers are focusing on relatively shallow water less than 50 m deep. For turbine arrays of the size we are discussing here, such depth restrictions will play an important role. For all the results, turbines are restricted to water deeper than 30 m, a reasonable minimum depth for 20 m in diameter turbines. It should be noted that the power calculations do not consider the asymmetry in the water speed between the flood and ebb tides or the possible changes in the direction of the flow. And, we have not accounted for the spring–neap cycle of the tides. All of these factors will change the exact power numbers calculated. Depending on the turbine design, they could result in either increases or decreases in power.

The results of the Tidal Array Model are shown in Fig. 2.25, where the turbine power is plotted versus the number of turbines. Three curves are plotted. The first has no restriction on the water depth where turbines can be placed. For the other two curves, turbines are

restricted to water depths of less than 70 m and 50 m. Considering the unrestricted-depth curve first, we see that the initial turbines produce a high rate of power. As the number of turbines increases, the power produced per turbine drops. So, for the first 500 turbines, each turbine produces about 1.5 MW, for the next 500 turbines each produces about 1 MW, and for greater than 2000 turbines each turbine is only adding about 0.5 MW. This just reflects the fact that the initial turbines are placed in locations where the water speed exceeds the average speed, while when we have already placed 2000 turbines, the turbines are being placed in locations of lower flow, often less than the average speed. It should also be noted that the turbines are restricted to the bottom, so that the majority of the channel cross-section is not a possible turbine location. However, it is still possible to achieve 2000 MW of power with a large array of nearly 2500 turbines. When there are 2000 turbines, the blockage ratio of the 200 strips has an average of 0.05 and a maximum of 0.1. If the power curve is compared to the results of the previous section, in particular Fig. 2.18, we see that the power produced is very similar to the curves for the blockage ratios of 0.05 and 0.1. The biggest difference is how the power per turbine changes as more turbines are added.

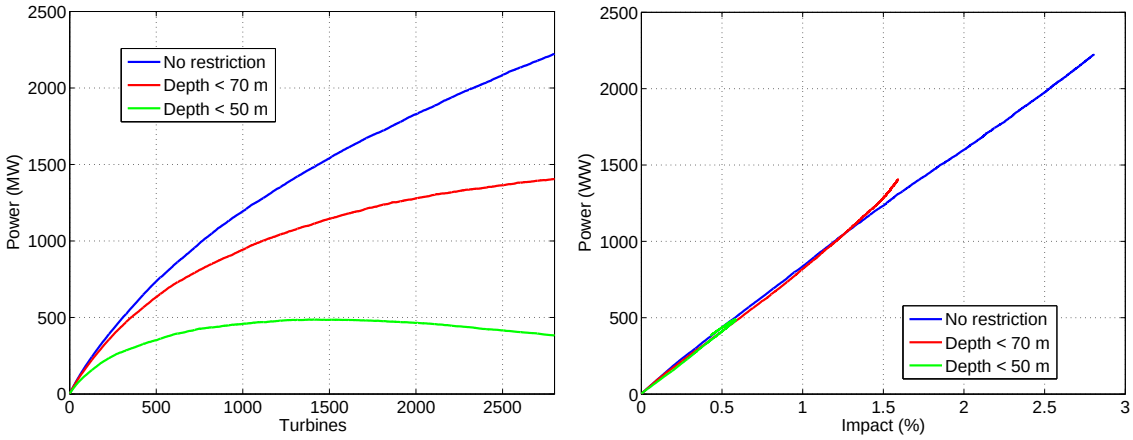

Figure 2.25: (Left) The total turbine power (MW) versus the number of turbines using the Turbine Array Model with $C_D = 1$. The top curve places no restriction on the water depth where turbines can be placed. The lower curves restrict turbines to water depths of less than 70 m and 50 m, respectively. (Right) The total turbine power (MW) versus the reduction in flow through the passage using the Turbine Array Model with $C_D = 1$.

When the turbines are restricted to water depths less than 70 m, we see a reduction in power. This reduction is not significant for the first 1000 turbines, but becomes large for greater than 2000 turbines. In fact, deploying more than 2000 turbines results in only a small increase in power. At this point, any additional turbine is being placed in the wake of a previously placed turbine. Thus, not only is the turbine in a location of weak flow, but it reduces the power of the other turbines that now lie in the new turbine's wake. Quite simply, we have run out of space to place more turbines.

If the turbines are restricted to water depths less than 50 m, we see a drastic reduction

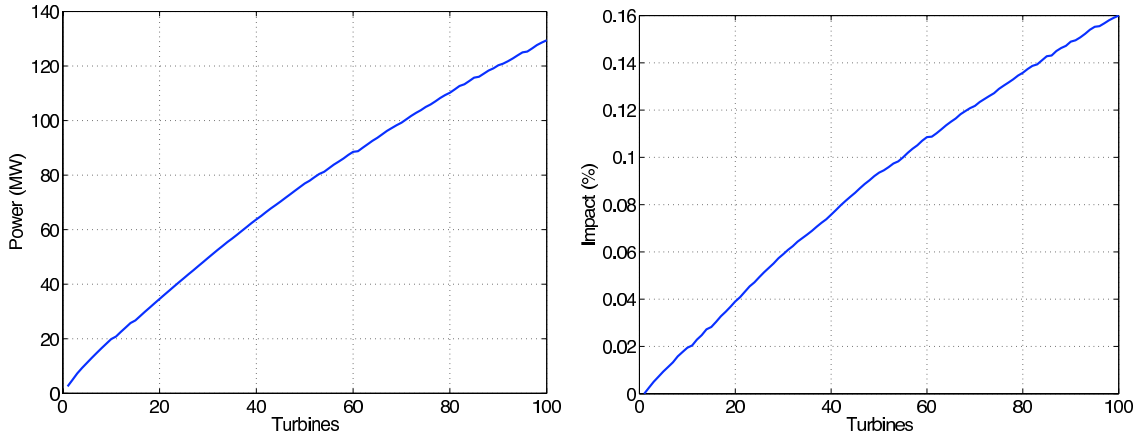

Figure 2.26: Left: The turbine power (MW) versus the number of turbines using the Turbine Array Model with $C_D = 1$. Right: The resulting reduction in flow through Minas Passage.

in the turbine power. This power reduction occurs immediately as there are few high-energy locations with a depth less than 50 m. The power increases very slowly after only 500 turbines and actually decreases after 1500 turbines, where the drag on the flow is still increasing but the turbines are so closely packed that they are all operating in another turbine's wake. It is clear from the last graph that being restricted to a maximum depth 50 m will severely restrict the power potential of bottom-mounted turbine arrays in Minas Passage. However, if we examine only the first 100 turbines, as shown in Fig 2.26, we see that they can generate significant power, more than 1MW per turbine. Therefore, the initial turbine arrays can be placed in shallow water.

In Fig. 2.25 we also plot the turbine power versus the reduction in flow for the three depth restriction cases. For all three cases the curve is a remarkably straight line, with 800 MW of power for every 1% reduction in flow. This is a slightly higher value than was seen in Fig. 2.17. For no depth restriction, 2000 MW of power extraction causes only a 2.5% reduction in flow. As well, Fig 2.26 emphasizes that for small arrays, the impact on the flow will be a fraction of a percent reduction in flow. Such small changes will be very difficult to observe given large natural variations. Once again, this reinforces the conclusion that a large quantity of turbine power is possible with little reduction in flow through the channel.

Finally, we examine the impact of changing the drag of the turbines. Fig. 2.17 suggests that the power could be increased by increasing the drag to above the Betz value of 1, but this increase would also increase the impact on the flow. In Fig. 2.27 we plot the turbine power versus the reduction in flow for 2000 turbines and a drag value varying from 0.7 to 1.9. The figure illustrates that both the power and the reduction in flow change by only a small amount over this range of drags, less than 100 MW and 1%, respectively. The power can be increased only a very small amount by increasing the drag beyond the Betz value of 1, but the power drops rapidly if the drag is made too large. In conclusion, there is little reason to tune the turbines to have a higher drag coefficient.

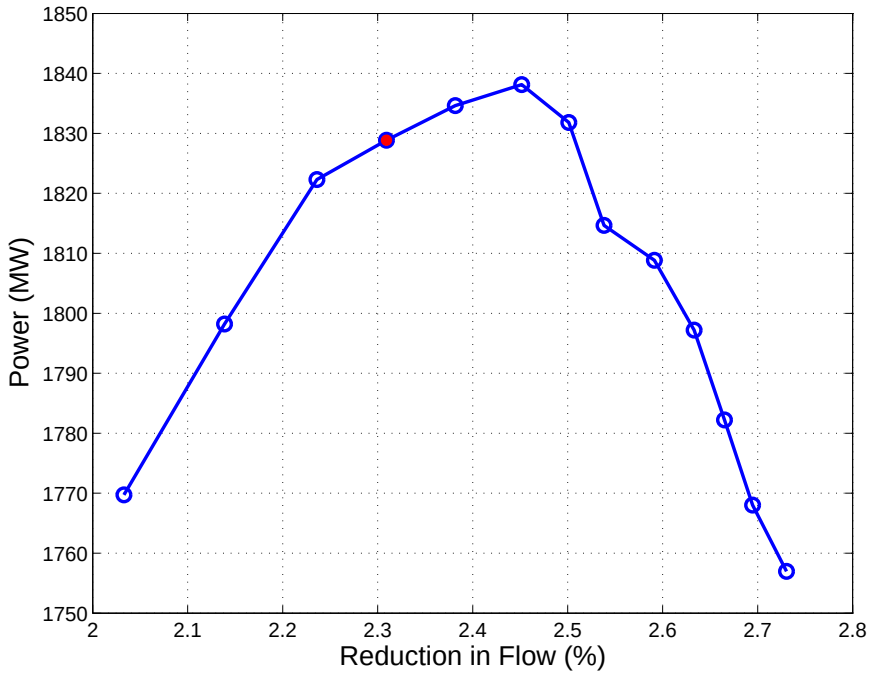

Figure 2.27: The total turbine power (MW) versus the reduction in flow through the passage using the Turbine Array Model with 2000 turbines. Each dot represents a different value of the turbine drag coefficient, varying by 0.1 from 0.7 on the right to 1.9 on the left. The solid red dot corresponds to $C_D = 1$, the value used in Figs. 2.25.

2.5 Outstanding Issues

Although our research project has accomplished the considerable results discussed above, we have not completed several important aspect of the initial proposal. In the initial proposal, we proposed to modelling the extraction of power using tidal lagoons. We did not pursue this research for several reasons. First, after some initial research into tidal lagoons we determined that modelling tidal lagoons would require considerable grid adaptation to examine a single specific lagoon. Thus a full examination of different lagoons would require a large part of the projects resources. Since another OEER project (Cornett) was examining the question and had made considerable progress, it seemed a waste of our resources to repeat their efforts. As well, there was limited interest in modelling lagoons from the majority of tidal energy stakeholders. A proper comparison of in-stream turbines and lagoon technologies is still required.

Second, in our proposal we described running long term simulations to estimate annual power production from locations. We also proposed running the model under extreme conditions to estimate the impacts of storm surges and sea level change. We have completed month long simulations that illustrate the spring-neap cycle of the tides. We have also used these simulations to make estimates of annual power production, and the variations of power over the year, see for example Fig 2.19. However, we have not published these results for a couple of reasons. First, as described in our research above, we still have several outstanding issues with our numerical model. While we have completed an initial validation of our model, we continue to work on the formulation a spatially varying bottom roughness to correspond to the differences seen in the observations. Such a formulation, should produce a more accurate model that will better model the variations in the vertical profile of the flow. Second, we do not have a complete understanding of what will cause the extreme tidal currents. We know from the ADCP observations, that tidal currents have large fluctuations at almost all times and all locations. We know that waves can affect the currents, but this has not been quantified for flows in Minas Passage. And, we know that weather events will effect the currents, but we don't have observations that correlate to changes in tidal currents to storm effects. Without a better understanding of these features, predictions of extreme tidal currents would be based solely of tidal harmonic analysis that, while useful, could lead to some poor conclusions.

Finally, in our proposal we expected to improve our numerical modelling of turbines substantially by the end of the project. We did make progress in extending our 2D model of turbines to 3D simulations, at least for fences of turbines. But, as shown in our comparison of the theory of partial fences to the simulations, their is a discrepancy that we do not understand. At the same time, the research into modelling turbines and the impact they have on the flow has progressed slowly over the past year. Considerable research is being done on this topic and progress is being made, for example the EWTEC 2011 conference this fall had many presentations on CFD modelling of turbines and turbine wakes. We are also working on refining our model by working with the developers of FVCOM on representing the impact of turbines in the turbulent kinetic energy equation and through our collaboration on another OEER funded research project.

Chapter 3

Dissemination and Technology Transfer

The research described in this report has been communicated to stakeholders in a number of ways. The Additional Information chapter gives a complete listing of all publications, presentations and other activities related to this project. Because of the timeliness of the topic, we have focused on presenting our results at conferences and in conference proceedings. In particular, we have published the majority of our results in three refereed conference proceedings in the past year. These articles were submitted to well respected international conferences. As well, results of this project were part of two undergraduate honours theses and will be included in an MSc thesis expected to be completed in the coming year. Finally, two other papers on different topics benefited from the research conducted in this project. It is expected that several more papers will be published on our ongoing research in the next year.

In addition to publishing, we have presented our results at over 20 conference and workshop presentations. Most of these have been oral presentations, with a few poster presentations. Presentations have been given by all members of the group, including the students. These presentations include the most of the important regional and national gatherings. They also include several international presentations at international conferences in the U.S., U.K., Europe, and Korea. Our research group has been active in regional and national workshops, both in giving presentations and acting as facilitators. We have made public presentations to community groups, teachers and students.

As well, Drs. Karsten and Culina have met and discussed our research with several turbine manufacturers and tidal energy developers, including Nova Scotia Power/Emera, Marine Current Turbines, Open Hydro, Fundy Tidal, New Energy Inc., and Ocean Renewable Power Company. We have visited several other universities where tidal research is taking place, including the University of Maine, University of Edinburgh, the University of Washington, the University of Victoria, as well as a visit to the European Marine Energy Center.

In the following weeks, our group in collaboration with the Fundy Energy Research Network will establish an data sharing ftp site. The results from this research project including data from numerical simulations will be made publicly available at this site. We have also

made a commitment to share the results of our numerical simulations with other researchers. Three members of the research group sit on the FERN subcommittee for hydrodynamics and geophysics.

Members of the research group were actively involved in research workshops and forums. Dr. Karsten served on the steering committee of the national Marine Technology Roadmap and has been assisting the Canadian representatives on IEC committee developing standards for power performance assessment of electricity producing tidal energy converters. And, Dr. Karsten is consulting with the department of education on including more aspects of tidal energy in the Nova Scotia Science curriculum.

Overall, we have been very active in disseminating our research and, in particular, communicating our results to the tidal energy community.

Chapter 4

Conclusions and Recommendations

Our research project has led to several interesting conclusions. In short, our goal in this research was to see whether the results of KMLH that suggested 2500 MW of power could be extracted from Minas Passage with only a 5% change in the flow through the passage would change significantly if we improved the numerical simulations of flow through Minas Passage and examined models of turbine fences and arrays rather than a full barrage like fence.

A closer examination of observations through analysis of ADCP measurements revealed that there is significant spatial heterogeneity in the values of the bottom friction coefficient C_D, and hence in the values of the bottom stress, that is not reflected in model output. The bottom boundary is particularly important in tidal flows because of the the logarithmic layer velocity profile reaches up through most of the water column, implying that the current magnitude is locally determined up to the height of this layer by the magnitude of the bottom stress. It is thus imperative to the accurate modelling of the current magnitude Minas Passage that the bottom friction coefficient be accurately inputted. As well, this analysis implies that the effects of tidal turbines placed on the sea-bed (e.g., those with a gravity base foundation) will be transmitted through to the top of the water column.

In comparing models with different grid resolutions, the current speeds on the high-resolution grid are significantly lower than the speeds on the low-resolution grid. Despite these mostly uniform reductions in speed with an increase in resolution, current direction is not significantly changed through most of the Passage. A probable cause of the diminished current speed is the resolution of more smaller-scale structures/eddies on the high-resolution grid. These eddies draw energy from the mean current, thereby reducing its speed. Indeed, the reduced power potential of Minas Passage from 8 GW with the low-resolution grid to 6 GW with the high-resolution grid is consistent with an increase in natural drag, as is confirmed by adjusting the natural drag parameter in the Garrett-Cummins formulation for power potential. However, the model sensitivity to resolution will be important for addressing issues on array scales and on smaller scales. Accurate representation of the boundary values (including bathymetry) and higher-resolution models, along with more detailed observations of the currents, will be needed to accurately determine the hydrodynamics in the Minas Passage on turbine-array

We have presented the results of a 3D numerical simulation of the flow through Minas Passage that clearly show the strong flow through the passage, supporting the idea that it is a very promising site for tidal power development. The simulations also illustrate the asymmetry between the flood and ebb tides and the significant vertical and cross-passage structure of the flow. This suggests that the potential power of the channel cannot be assessed using theories that assume the flow is uniform. Increasing the horizontal resolution also clearly defined regions of high eddy activity, such as Cape Split.

We have derived an adaption of previous theory presented by Vennell [21] that combined the LMADT of Draper et al. [18] with the theory of KMLH to examine the potential power generation of turbine fences and arrays in Minas Passage. The results show that fences with a larger blockage ratio produce more power especially if they are designed to have a higher drag. But, such fences can be less efficient and they have a larger impact on the flow. The theory suggests that the turbine drag can be tuned to balance the trade-off between generating more power and having a larger impact on the environment through the resulting reduction in flow. We also extended this model to a Turbine Array Model, which took into account the variations in flow in the passage, turbine wakes, and the positioning of turbines. The overall conclusion is the results of KMLH are supported. In both models, over 2000 MW of turbine power could be generated by an array of 2000 turbines with less than a 5% reduction in the flow. For smaller arrays, 700 to 800 MW of power is possible for every 1% reduction in the flow.

Several other conclusions come out of our array analysis. For a channel the size of Minas Passage, the blockage ratios will be very low, generally less than 0.1. So the importance of the LMADT theory is reduced and there is little reason to tune the turbines to have a higher drag coefficient. The predicted change in the flow through the passage is so small (see Fig 2.26), that it does not need to be accounted for in the power assessment of small arrays. The Turbine Array Model results indicate that the most important aspect of assessing an array is locating the turbines in regions of high flow and not in each other's wakes. The model results also illustrate that if turbines are restricted to water depth less than 50 m, the size and potential power of the array will be severely restricted. Increasing the restricted depth to 70 m greatly increases the potential size and power of the array. But to achieve 2000 MW of power, either the turbines will need to be deployed in deep water or turbines that extract power from higher in the water column will also need to be deployed.

Finally, our 3D simulations of partial turbine fences as regions of increased drag did not agree well with the theory, producing maximum power three to six times too large. There are several reasons this may be the case, as both the theory and the simulations have some important limitations. One possibility is that because of the thickness of the simulated turbines, the flow moving around the turbines is able to accelerate the flow in the turbines, allowing for larger turbine drags and thus greater power. Another possibility is that the theory of partial turbine fences does not properly account for the natural drag on the flow around the turbines. Future work will focus on better representations of turbines in our numerical simulations to see if this discrepancy can be resolved.

The results we have found must be interpreted as initial results of ongoing research.

Obviously, there remains many questions that need answering. To improve our numerical models we need to better understand the bottom stress and its effect of the vertical velocity profile. One means of deriving an accurate bottom stress is to utilise acoustic backscatter data to infer bottom roughness values, from which bottom friction can be derived. A related avenue of future study will be to determine where in the water column turbines should be placed to maximise their efficiency. As well, our numerical models need to be higher resolution so that they can model the unsteady, turbulent flow seen in ADCP observations. At the same time, we need simulations that include wave forcing to examine the impact of regular waves and extreme events. Such models will need to be further validated against observations that are both short term - to quantify turbulence - and long term - to measure natural variation and extreme events. A well, greater spatial coverage of observations will be required. Several studies are underway to better observe turbulence in the flow. But other observational programs should be considered. The deployment of pressure sensors to measure the long term variations in sea surface elevation would give the long term observations required, while Very High Frequency radar could give high resolution measurements of currents over a large region of space.

The turbine power values presented here can easily be made more realistic by using the power curve of a specific turbine. For the energetic flow in Minas Passage, the most important aspect of the power curve is the speed at which the turbine regulates power. If this is low, the turbine will not be able to take advantage of the strongest flows and the power levels will decrease. However, if we are to examine turbine arrays it is critical that we understand the total power turbines extract from the flow. Not only is this important for designing an efficient array, it is vital for understanding the impact of the turbines on the flow.

We have also not addressed the question of whether it is actually possible to deploy turbines in the locations chosen for their high flow. For example, the sea bottom may not allow turbine installation. These details could strongly affect the design of the turbine and the choice of location to deploy the turbine. As well, the logistics and costs of installing, operating, and maintaining such a large turbine array need to be accurately estimated to determine if such arrays are economical. These questions are critical to making a valid site assessment for a turbine or an array of turbines. We believe greater effort should be put into site assessment that address all aspects of turbine deployment and operation.

Finally, our analysis has indicated that the impact of the turbines is small, in terms of reduction in the flow through Minas Passage. While this is an important measure of the impact, it is only the first step in assessing the impact of a turbine array. The impact of even small changes in the Minas Passage flow on the intertidal zones of Minas Basin still need to be examined and quantified. As well, the impact large arrays will have on the marine life that passes through Minas Passage is largely unknown.

It is important to remember that extracting hundreds of megawatts of power from Minas Passage will require hundreds of instream turbines. A small increase in a turbine's efficiency or a decrease in its impact on the environment could add up to significant changes for large arrays. Therefore, while significant progress has been made on assessing the potential of tidal

power in Minas Passage, we believe there remains significant work to be done in realizing this potential in a responsible way.

Bibliography

[1] Triton Consultants Ltd. Canada Ocean Energy Atlas (Phase 1) Potential Tidal Current Energy Resources Analysis Background, 2006.

[2] G. Hagerman, G. Fader, G. Carlin, and R. Bedard. EPRI Nova Scotia Tidal In-Stream Energy Conversion Survey and Characterization of Potential Project Sites. *December*, 2006.

[3] D. A. Greenberg. A numerical model investigation of tidal phenomena in the Bay of Fundy and Gulf of Maine. *Marine Geodesy*, 2(2):161–187, 1979.

[4] R.H. Karsten, J.M. McMillan, M.J. Lickley, and R.D. Haynes. Assessment of tidal current energy in the Minas Passage, Bay of Fundy. *Proceedings of the Institution of Mechanical Engineers, Part A: Journal of Power and Energy*, 222:493–507, 2008.

[5] C. Garrett and P. Cummins. The power potential of tidal currents in channels. *Proceedings of The Royal Society*, 461:2563–2572, 2005.

[6] J. Blanchfield, C. Garrett, P. Wild, and A. Rowe. The extractable power from a channel linking a bay to the open ocean. *Proceedings of the Institution of Mechanical Engineers, Part A: Journal of Power and Energy*, 222(A3):289–297, 2008.

[7] Changsheng Chen, Geoffery Cowles, and Robert Beardsley. An unstructured grid, finite-volume coastal ocean model: FVCOM User Manual, Second Edition. *SMAST/UMASSD Technical Report-06-0602*, page 315, 2006.

[8] J. Culina and R. Karsten. Comparison of Different Resolution Models and Observed Current Proles in the Bay of Fundy, Canada Using Turbine-Relevant Metrics. *Proceedings of the 9th European Wave and Tidal Energy Conference*, 2011.

[9] Zhigang Lai, Changsheng Chen, Geoffery Cowles, and Robert Beardsley. A nonhydrostatic version of FVCOM: 1. Validation experiments. *Journal of Geophysical Research-Oceans*, 115:21, 2010.

[10] Yongsheng Wu, Jason Chaffey, David Greenberg, Keir Colbo, and Peter Smith. Sediment transport patterns in the Bay of Fundy: a numerical study. *Under review*, 2011.

[11] Samuel Gooch. Siting methodologies for tidal in-stream energy conversion (TISEC) systems. pages 63, M.Eng. thesis, University of Washington, 2009.

[12] Brian Polagye and Jim Thomson. Tidal energy resource characterization: methodology and case study for Admiralty Inlet, Puget Sound, US. *In preparation*, 2011.

[13] Rolf Lueck and Youyu Lu. The logarithmic layer in a tidal channel. *Continental Shelf Research*, 17:1785–1801, 1997.

[14] Alan Elliott. The boundary layer character of tidal currents in the eastern Irish Sea. *Estuarine Coastal and Shelf Science*, 55:465–480, 2002.

[15] C. Garrett and P. Cummins. The efficiency of a turbine in a tidal channel. *Journal of Fluid Mechanics*, 588:243–251, 2007.

[16] J.I. Whelan, J.M. Graham, and J. Peiro. A free-surface and blockage correction for tidal turbines. *Journal of Fluid Mechanics*, 624:281–291, 2009.

[17] G.T. Houlsby, S. Draper, and M. Oldfield. Application of linear momentum actuator disc theory to open channel flow. *Technical Report 2296-08, OUEL*, 2008.

[18] S. Draper, G.T. Houlsby, M.L.G. Oldfield, and A.G.L. Borthwick. Modelling tidal energy extraction in a depth-averaged coastal domain. *Proceedings of the 8th European Wave and Tidal Energy Conference*, 2009.

[19] G.P. Corten. Flow separation on wind turbine blades. *PhD Dissertation, Universiteit Utrecht, Netherlands*, 2001.

[20] R. Karsten, A. Swan, and J. Culina. Assessment of Arrays of In-stream Tidal Turbines in the Bay of Fundy. *Proceedings of the 9th European Wave and Tidal Energy Conference*, 2011.

[21] R. Vennell. Tuning Turbines in a Tidal Channel. *J. Fluid Mechanics*, 663:253–267, 2010.

Chapter 5

Additional Information

5.1 Publications

Papers Published in Refereed Journals

1. P. Ranjan, R. Haynes, and R. Karsten, 2010, "Gaussian Process Models and Interpolators for Deterministic Computer Simulators," *Technometrics* in press.

2. Patrick F. Cummins, Richard H. Karsten, Brian K. Arbic, 2010, "The Semi-Diurnal Tide in Hudson Strait as a Resonant Channel Oscillation," *Atmosphere Ocean* , **48**, 163–176.

Refereed Conference Proceedings

1. J. Culina and R. Karsten, "Comparison of Different Resolution Models and Observed Current Proles in the Bay of Fundy, Canada Using Turbine-Relevant Metrics" Proceedings of the 9th European Wave and Tidal Energy Conference, 5–9 September, 2011, Southampton, U.K.

2. R. Karsten, A. Swan, and J. Culina, "Assessment of Arrays of In-stream Tidal Turbines in the Bay of Fundy", Proceedings of the 9th European Wave and Tidal Energy Conference, 5–9 September, 2011, Southampton, U.K.

3. Richard H. Karsten, 2011, "An Assessment of the Potential of Tidal Power from Minas Passage, Bay of Fundy, Using Three-Dimensional Models," Proceedings of ASME 2011 30th International Conference on Ocean, Offshore and Arctic Engineering, June 19–24, 2011, Rotterdam, Netherlands.

4. Greg Trowse and Richard Karsten, "Bay of Fundy Tidal Energy Development- Opportunities and Challenges," Proceedings of the 3rd International Conference on Ocean Energy, 6–8 October 2010, Bilbao, Spain.

Conference Proceedings

1. Richard H. Karsten, Justine M. McMillan, Megan J. Lickley, and Ronald D. Haynes, 2009: "A Review of a Recent Assessment of Tidal Current Energy in Minas Passage, Bay of Fundy." in **Resource Development and its Implications in the Bay of Fundy and Gulf of Maine, proceedings of the 8th BoFEP Bay of Fundy Science Workshop.** 15–22.

Theses

1. Amber Corkum, "Particle Swarm Optimization Applied to Tidal Turbine Placement in the Minas Passage", Undergraduate Honours Thesis, Department of Mathematics and Statistics, Acadia University, April 2011.

2. Amanda Swan, "Modelling Power Output for Tidal Turbines", Undergraduate Honours Thesis, Department of Mathematics and Statistics, Acadia University, April 2011.

Conference Presentations:

1. Amber Corkum, "Particle Swarm Optimization Applied to a Tidal Power Problem", Atlantic Provinces Council on the Sciences Computer Science, Mathematics and Statistics Undergraduate Conference, Halifax, October 16, 2010.

2. Amber Corkum, "Optimization Strategies for Tidal Turbine Power", Atlantic Provinces Council on the Sciences Computer Science, Mathematics and Statistics Undergraduate Conference, Halifax, October 23, 2009.

3. Amanda Swan, A Model of Power Output for Tidal Turbines, Atlantic Provinces Council on the Sciences Computer Science, Mathematics and Statistics Undergraduate Conference, Halifax, October 16, 2010.

4. Amanda Swan, Optimizing Tidal Power Potential in the Bay of Fundy, Atlantic Provinces Council on the Sciences Computer Science, Mathematics and Statistics Undergraduate Conference, Halifax, October 24, 2009.

5. Joel Culina, Assessment of tidal current energy in the Minas Passage, Bay of Fundy, CMOS Annual Meeting, June 4, 2010, Ottawa, ON.

6. D. Greenberg, F. Lyard and Z. Wang - TUGOm - progress, application and testing. International workshop on Multiscale (Un)-structured mesh numerical ocean Modeling, MIT, Cambridge, MA, 17-20 August 2010 (this involved comparisons of models (including FVCOM) in highly non linear flows.)

7. David Greenberg, Flow acceleration and separation tests for nonlinear models, CMOS Annual Meeting, June 4, 2010, Ottawa, ON.

8. David Greenberg, Models and data for tidal power studies, Atlantic Geoscience Society, February 6, 2010, Wolfville, NS.

9. David Greenberg, Bay of Fundy Tides - Past Present Future, Dalhousie University Physical Oceanography and Meteorological Seminar Series, December 3, 2009, Halifax, NS.

10. Richard Karsten, "Assessing the In-Stream Power Potential of Tidal Currents in the Bay of Fundy," Korea Green Technology and Industry Exhibition 2011, November 9, 2011, Incheon, Korea.

11. Richard Karsten, "Putting tidal energy development in perspective," OREG 2011 Annual Conference: A Time to Lead, November 2, 2011, Montreal, QC.

12. Richard Karsten, "An Assessment of the Potential of Tidal Power from Minas Passage, Bay of Fundy, Using Three-Dimensional Models," Proceedings of ASME 2011 30th International Conference on Ocean, Offshore and Arctic Engineering, June 22, 2011, Rotterdam, Netherlands.

13. Richard Karsten, "Tidal Power in the Bay of Fundy," Renewable Energy Conference, April 20th, 2011, Halifax, NS.

14. Richard Karsten, "Assessment of tidal current energy in the Bay of Fundy," Canadian Symposium for Fluid Dynamics/CAIMS 2010, June 20, 2010, St. Johns NL.

15. Richard Karsten, "Assessment of the Potential of Tidal Power from Minas Passage and Minas Basin," NS Energy R&D Forum 2010, Halifax, NS, May 26, 2010.

16. Richard Karsten, "Assessment of Tidal Current Energy," Atlantic Geoscience Society, February 6, 2010, Wolfville, NS.

17. Richard Karsten, "Assessment of Tidal Current Energy," Conference on Clean Energy, November 12, 2009, Boston, MA.

18. Richard Karsten, "Assessment of Tidal Current Energy in the Minas Passage, Bay of Fundy," OREG 2009 Fall Symposium: Ocean Energy in Ottawa, October 28, 2009, Ottawa, ON.

19. Richard Karsten, "Modelling Tidal Power in the Minas Passage", APICS Mathematics, Statistics and Computer Science Joint Conference, October 2009, Halifax, NS.

Workshops Presentations

1. Richard Karsten, "Tidal Power in the Bay of Fundy", Ocean Industry/University Workshop, June 2, 2011, Halifax.

2. Richard Karsten, "Resource Assessment", Coastal Community Forum, Acadia, August 17, 2011.

3. Richard Karsten, "Assessment of the Potential of Tidal Power from Minas Passage and Minas Basin," OEER/FORCE Tidal Energy Workshop, October 13, 2010, Wolfville, NS.

4. Richard Karsten, "Assessment of the Potential of Tidal Power from Minas Passage and Minas Basin," Offshore Energy and Environmental Research Information Sharing Session, January 29, 2010, Dartmouth, NS.

Poster Presentations

1. Richard Karsten, "Assessment of Arrays of In-stream Tidal Turbines in the Bay of Fundy", Proceedings of the 9th European Wave and Tidal Energy Conference, September 7th, 2011, Southampton, U.K.

2. Amber Corkum, Optimization of Turbine Location, NS Energy R&D Forum 2010, Halifax, NS, May 26, 2010.

3. Mitchell O'Flaherty-Sproul, "Particle Tracking through Minas Passage," NS Energy R&D Forum 2010, Halifax, NS, May 26, 2010.

4. Amber Corkum, and Amanda Swan, "Optimization of Tidal Turbine Power", Canadian Applied and Industrial Mathematics Society Conference July 17-21, 2010.

5. Mitchell O'Flaherty-Sproul and Richard Karsten, "Particle tracking through Minas Passage", Canadian Applied and Industrial Mathematics Society Conference July 17-21, 2010.

Invited Seminars

1. Richard Karsten, University of Maine, Orono, ME, Sept. 23, 2011.

2. Richard Karsten, "Assessment of the Potential of Tidal Power from Minas Passage and Minas Basin," Bedford Institute of Oceanography, Dartmouth, NS, March 5, 2010.

Community Talks

1. Richard Karsten,"The Science of Tidal Power", Nova Scotia Association of Science Teachers Annual Meeting, October 28, 2011

2. Richard Karsten, "Tidal Power in the Bay of Fundy", Acadia Research Summit, Acadia University, March 24, 2011.

3. Richard Karsten,"The Science of Tidal Power", Nova Scotia Association of Science Teachers Annual Meeting, October 22, 2010

4. Richard Karsten,"Sustainable Tidal Energy Research and Development", Tidal Energy in Digby County, Brier Island, Nova Scotia, August 24, 2010.

5. Richard Karsten and Mitchell O'Flaherty-Sproul, "Harvesting Tidal Energy from the Bay of Fundy, Academy for the Environment and ACER Great Debate", Wolfville, March 31, 2010.

6. Richard Karsten, "Turning High Tides into Green Energy," Atlantic Undergraduate Physics and Astronomy Conference, Wolfville, February 7, 2010.

Guest lectures

1. Richard Karsten,"Assessment of tidal current energy in the Bay of Fundy", Saint Mary's University , February 16, 2011.

2. Richard Karsten,"Assessment of tidal current energy in the Bay of Fundy", Acadia University , October 16, 2011.

Workshops Participation

1. Richard Karsten, Getting Power to Market, July 7-8, 2011, Halifax, NS.

2. Richard Karsten, Canada's Marine Renewable Energy Technology Roadmap Workshop 3, June 8–9, 2011,Vancouver, BC – Breakout Session Facilitator.

3. Richard Karsten, Canada's Marine Renewable Energy Technology Roadmap Workshop 2, March 29–30, 2011, Montreal QC – Breakout Session Facilitator.

4. Richard Karsten, Canada's Marine Renewable Energy Technology Roadmap Workshop 1, February 8, 2011, Halifax NS – Breakout Session Facilitator.

5. Many members of our team were involved in the OEER/FORCE workshop held in Wolfville. Drs Karsten and Greenberg acted as Session Chairs for two of the three Workgroups. Mitchell O'Flaherty-Sproul was a recorder for one of the sessions.

Other Dissemination Activities

1. Dr Karsten and M. Tarbotton participated in a conference call discussing the development of tidal power in B.C. M. Tarbotton and Dr Culina participated in the follow up meeting meeting on resource assessment and modelling of Johnstone Strait held prior to OREG meeting.

2. Dr Culina attended the OREG conference in Vancouver.

3. While staying in Victoria, Dr Culina met with Dr. Roy Walters and Mr. Clayton Hiles (Triton), Dr. Mike Foreman (DFO), Drs. Curran Crawford, Adam Monahan (UVic) and Drs. Brian Polagye, Jim Thomson and Mitsuhiro Kawase (U.Wash).

4. Dr Karsten is serving on Mirror Committee which provides Canadian input to the committee writing the Power Performance Assessment of Tidal Energy Converters Standards document for the International Electrotechnical Commission.

5. Dr. Karsten is a steering committee member developing the Marine Renewable Energy Technology Roadmap for Canada

6. Dr. Karsten is co-chair of FERN's Hydrodynamics and Geophysics Sub-Committee. Drs Greenberg and Culina are committee members.

7. Dr. Karsten made his tidal power research part of a presentation at Open Acadia day.